Model and Characterization of a Passive Biomimetic Ankle for Lower Extremity Powered Exoskeleton

Brandon Fournier

Thesis submitted in partial fulfillment of the requirements for the

MASTER OF APPLIED SCIENCE DEGREE

in Biomedical Engineering

Ottawa-Carleton Institute for Biomedical Engineering
University of Ottawa
Ottawa, Ontario

April 2018

Abstract

Lower extremity powered exoskeletons (LEPE) allow people with spinal cord injury (SCI) to perform activities of daily living, such as standing, walking, or stair and ramp ascent/descent. However, current LEPE walk slowly and require extensive use of forearm crutches to maintain user stability. Consequently, this limits LEPE time of use and overall system performance. While the biological ankle is known to be critical for energy efficiency, speed, and stability in able-bodied walking, current LEPE do not include biomimetic ankle designs and thus limit device performance.

The objective of this thesis is to determine biomimetic ankle mechanics for a LEPE, thereby defining ankle design requirements that could reduce crutch loads and thus extend LEPE use. Virtual prototyping techniques were used to achieve this objective. Two 3D models of a real LEPE (ARKE, Bionik Laboratories) attached to a human musculoskeletal model were developed and validated. The first model (biomimetic model) was driven by 3D marker kinematics from 30 able-bodied participants walking at four realistically slow LEPE walking speeds. The second model (SCI model) was driven by 3D marker kinematics from five SCI participants walking in the ARKE LEPE with instrumented forearm crutches. Once the models were validated by comparing predicted to measured ground reaction forces (GRF) and centre of pressure (COP) trajectories, biomimetic LEPE ankle design requirements were determined.

Ankle range of motion, quasi-stiffness, work, peak moment, and peak power were compared between human and human+ARKE models, across four gait phases and four slow walking speeds. The major findings were: the human+ARKE model had significantly different quasi-stiffness values across all four gait phases; quasi-stiffness increased with increasing speed; the human+ARKE model's ankle always absorbed net-work, even at the fastest walking speed; quadratic regression was significantly more accurate than linear regression for modelling ankle quasi-stiffness. These results suggested that passive variable stiffness ankles incorporating quadratic elastic spring elements could achieve biomimetic ankle functions and thus potentially increase LEPE user walking speed, stability, and reduce overuse of crutches.

Table of Contents

Table of Figures

List of Tables

Definitions

Anterior	To the front of the body
Centre of mass	Point representing the mean position of mass of a body
Concentric Contraction	Muscle contraction where the muscle shortens
Distal	Away from the rest of the body
Dorsal	Posterior surface
Dorsiflexion	Foot rotation towards the knee
Eccentric contraction	Muscle contraction where the muscle lengthens
Electromyography	Technique for measuring electrical activity of muscles
Extension	Joint rotation causing an increase in angle
External moment	Moment applied from outside the body
Flexion	Joint rotation causing a decrease in angle
Gait cycle	Cycle of walking
Force platform	Equipment for measuring ground reaction forces
Frontal plane	Divides the body into front and back portions (also referred to as coronal plane)
Ground reaction force	Reaction force from the ground applied to the foot
Internal moment	Moment generated by muscles and/or ligaments
Internal rotation	Rotation of limb about its long axis, the anterior surface moving medially
Kinematics	Movement of joints or body segments
Kinetics	Forces and moments that produce movement
Lateral	Away from the midline of the body
Medial	Towards the midline of the body
Orthosis	External support for some part of the body
Plantarflexion	Foot rotation away from the knee
Posterior	To the back of the body
Prosthetic limb	Artificial limb
Proximal	Towards the rest of the body
Power	Rate at which work is done or energy is expended
Sagittal plane	Divides the body intro right and left portions
Stance	Phase of gait cycle when foot is in contact with the support surface
Step	Foot strike of one extremity to foot strike of the opposite extremity

Stride	Foot strike of one extremity to next foot strike of the same extremity
Swing	Phase of gait cycle when foot is not in contact with the support surface
Transverse plane	Divides the body into upper and lower portions

Abbreviations

AFO	Ankle-foot orthosis
AMS	Anybody Modelling System
COM	Centre of mass
COP	Centre of pressure
DoF	Degrees of freedom
EMG	Electromyography
GRF	Ground reaction force
HAT	Head, arms, and trunk
HKAFO	Hip-knee-ankle-foot-orthosis
KAFO	Knee-ankle-foot orthosis
LEPE	Lower extremity powered exoskeleton
ROM	Range of motion
RTL	Rehabilitation Technology Lab
SCI	Spinal cord injury
TOHRC	The Ottawa Hospital Rehabilitation Centre

Acknowledgments

First of all, I would like to thank my two supervisors Dr. Edward Lemaire & Dr. Marc Doumit for all of their guidance, support, and encouragement throughout my research.

I would also like to thank Bionik Laboratories and Ontario Centres of Excellence for funding this research.

A thank you also goes out to the following individuals:

Staff of Anybody Technology A/S
Mohammad Shourijeh

Andrew Smith
Drew Herbert-Copley
Johnny Farah

Finally, thank you to my family and friends.

Chapter 1: Introduction

1.1 Introduction

Current lower extremity powered exoskeletons (LEPE) allow people with spinal cord injuries (SCI) to stand, walk, and sometimes ascend and descend stairs, thus increasing their independence and quality of life. Most designs have electrically actuated hips and knees, require extensive use of forearm crutches, and have simplistic ankle designs that focus on foot clearance. This is in stark contrast with biomechanics literature showing that, in healthy individuals, ankle mechanics are quite complex and are responsible for a number of important mobility features such as energy efficiency, momentum control, walking speed, and stability. For normal and slow walking speeds, the ankle provides a significant portion of the propulsive power. Furthermore, the most substantial component of frontal plane walking stability is sagittal ankle power modulation. Lack of proper ankle function may increase the energy requirements from exoskeleton knees and hips, as well as crutch overuse that leads to user fatigue, thereby limiting continuous exoskeleton use before a rest period is required.

To determine optimal mechanical properties for a biomimetic exoskeleton ankle, the ARKE powered exoskeleton (Bionik Laboratories) was modeled in the AnyBody musculoskeletal modelling software. 3D marker data were collected from healthy individuals as they walked slowly and this data drove the kinematics of a combined human and ARKE model. This simulation produced joint kinetics, thus delivering ARKE ankle mechanical properties that produced crutch-free healthy motion.

In this thesis, requirements for a biomimetic LEPE ankle, suitable for ARKE, were determined through simulation using AnyBody modelling software. First, models of a human wearing the ARKE were generated and validated. Second, biomimetic LEPE ankle mechanics were characterized and design recommendations were made.

1.2 Rationale

Current LEPE walk very slowly and users can become fatigued quite rapidly, likely due to overuse of crutches. Since most current LEPE have simplistic ankle designs with low functionality, compared to biological ankles, these shortcomings could be addressed with better ankle designs. Furthermore there is a dearth of literature pertaining to healthy ankle mechanics applied to the field of powered exoskeletons.

Considering these two points, it is important to study the mechanics that describe LEPE ankle design that can match healthy biological ankle function. Instead of iteratively building

prototypes of inspired ankle designs and comparing them to healthy ankle function, to achieve this objective, a cost and time effective approach would involve computer simulations of healthy motion of a human wearing a LEPE.

Furthermore, a full 3D model of a human and real LEPE, including interaction forces, could be used and modified for future research on LEPE biomechanics and design improvement.

1.3 Objectives and hypotheses

This thesis developed and evaluated a combined human-LEPE model and used the model to determine biomimetic ankle requirements for LEPE walking. The three objectives were:

1) Generate and evaluate the validity of a combined "human musculoskeletal and LEPE" biomimetic model for different slow walking speeds.

   Hypothesis:

   a. The model will satisfactorily replicate measured ground reaction forces.
   b. Model ground reaction force accuracy will increase with walking speed.

2) Validate a model that simulates motion of spinal cord injured participants using the ARKE.

   Hypothesis:

   a. The model will satisfactorily replicate ground reaction forces.

3) Determine biomimetic ankle requirements of the ARKE LEPE for different walking speeds.

   Hypothesis:

   a. Ankle will absorb net energy for all speeds and ankle stiffness will increase with walking speed.
   b. Ankle mechanical properties while wearing the ARKE will be different from human only ankle properties when not wearing ARKE.

1.4 Contributions of the thesis

The principal contribution of the thesis was creating and validating a human and ARKE LEPE model that can be used to study powered exoskeleton designs and their effects on the human. For the first time, a LEPE+human model that incorporates interactions between LEPE and person was validated for realistic LEPE speeds. Also, for the first time, a simulation of LEPE-human interaction was developed that includes crutches and is driven by 3D motion capture data from SCI users actually wearing the LEPE. This thesis also provides a description of LEPE ankle mechanics required for healthy walking through simulation. Simulations have shown that current designs fall short of providing biomimetic mechanics and thus may lead to very slow walking and compensation through crutches over use.

1.5 Thesis Outline

This thesis is in manuscript format and is divided into 5 chapters. Chapter 2 is a literature review covering healthy biological ankle mechanics, the state of the art in ankle-foot prosthetics, orthotics, biped robots, and LEPE, as well as a section on exoskeleton model simulations. Chapter 3 presents a submitted journal manuscript that describes and validates two models, one biomimetic LEPE-human model that was driven by able-bodied very slow walking motion and a second SCI model of the LEPE-human that included crutches and was driven by motion from SCI users actually wearing the ARKE LEPE. Chapter 4 presents a submitted journal manuscript investigating biomimetic ankle requirements for walking in the ARKE LEPE at realistic slow exoskeleton speeds using a full 3D model of ARKE attached to a musculoskeletal human model in the Anybody Modelling System. Chapter 5 consists of a thesis summary, LEPE ankle design recommendations, and suggestions for future work.

Chapter 2: Literature Review

This chapter reviews biological ankle/foot mechanics and the state of the art for ankle mechanisms in biped machines, to better determine requirements and gain insight for ankle/foot components in a LEPE for people with lower extremity paralysis.

2.1 Ankle/Foot Anatomy

2.1.1 Bones

The foot contains 26 bones (Figure 2-1). The fibula stabilizes the ankle joint laterally, although it bears almost none of the body weight, which is transferred almost exclusively via the tibia. The calcaneus consists of the heel and hindfoot structures while the talus is used as a pivot for multiple ankle/foot joints. The tarsals and metatarsals form the mid and forefoot, respectively, and the phalanges are the toe bones [1].

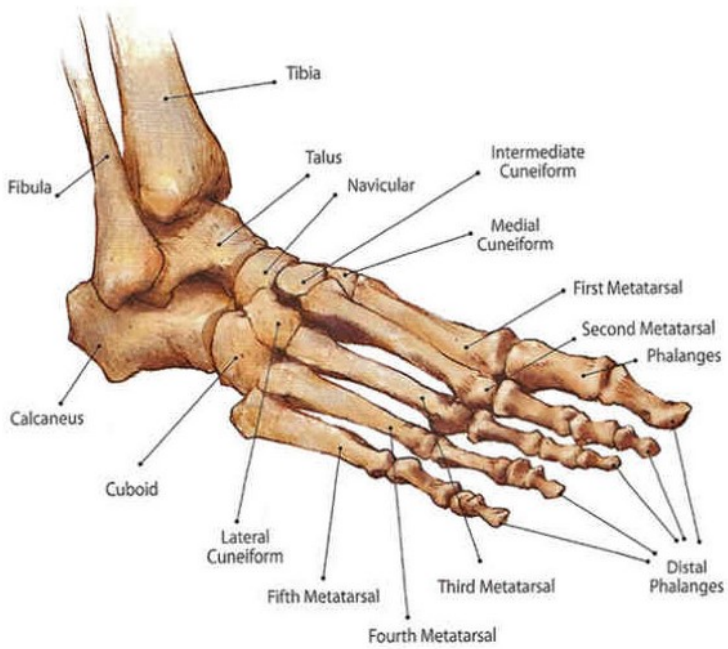

Figure 2-1 Foot and ankle bones (adapted from [2]).

2.1.2 Joints

The principal articulations in the ankle-foot complex are synovial joints. Synovial joints are covered by smooth cartilage to allow sliding between two bones with little friction. Friction is further

minimized by synovial fluid that lubricates the joint. The cartilage behaves viscoelastically, allowing small amounts of damping that helps minimize impact forces by absorbing energy.

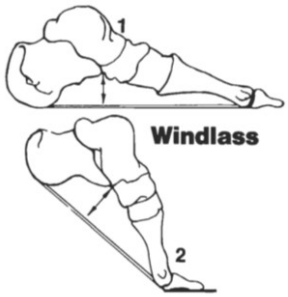

Figure 2-2 Windlass mechanism (adapted from [6]).

The tibiotalar joint allows dorsiflexion and plantarflexion, although joint movement is coupled to the subtalar joint (inversion and eversion). The tibiotalar joint allows the tibia to slide over the talus and can be modelled as a revolute joint. In neutral position, the joint axis is 20º externally rotated in the transverse plane and 10º rotated in the coronal plane such that the lateral side is most inferior. Therefore, ankle dorsiflexion is slightly everted and ankle plantarflexion is slightly inverted [3]. Tibiotalar joint range of motion (ROM) is typically 25º dorsiflexion to 41º plantarflexion [4].

Three principal joints are within the foot: subtalar, midtarsal, and metatarsophalangeal. The subtalar joint mainly rotates in the coronal plane (inversion and eversion) due to sliding of the talus over the calcaneus. Although, the axis of rotation is tilted 45º in the sagittal plane and 20º in the transverse plane [3]. Maximum inversion and eversion is approximately 16º [4]. The subtalar joint also allows considerable internal and external rotation of 20º. These transverse plane rotations occur during gait as a result of bone geometry and offset between body weight vector and ground reaction forces, creating a moment that rotates the ankle joint axis to allow only sagittal plane rotation (i.e., plane of forward progression) [3]. The midtarsal joint consists of the talonavicular and calcaneocuboid joints. The midtarsal joint couples arch height modulation to subtalar joint eversion and inversion, allowing foot compliance to change during gait [3]. The metatarsophalangeal joints allow toe plantar and dorsiflexion relative to the forefoot. Maximum dorsiflexion and plantarflexion are on average 76º and 34º, respectively [5]. Toe dorsiflexion is also coupled to midtarsal joint movement through the windlass mechanism (Figure 2-2). When toes dorsiflex the plantar aponeurosis tightens, pulling the calcaneus anteriorly and raising the foot's arch [6].

2.1.3 Muscles and Tendons

The 20 muscles in the ankle-foot complex can be divided into four groups: plantar flexor, dorsiflexor, inverter, and everter (Figure 2-3). Almost all muscles are both plantar or dorsiflexors, as well as inverter or everters. The triceps surae muscles consist of medial and lateral heads of the gastrocnemius and the soleus muscle, which is the largest muscle of the ankle-foot complex and is capable of creating the most torque. These muscles are mainly plantar flexors, but the soleus is also an inverter and the gastrocnemius is an everter. Gastrocnemius is a biarticulate muscle capable of plantar flexing the ankle and flexing the knee [3]. The two most significant dorsiflexor muscles,

although much weaker than plantar flexors, are the tibialis anterior and the extensor digitorum longus (EDL). Tibialis anterior is also an inverter and extensor digitorum longus is also a metatarsophalangeal dorsiflexor [3].

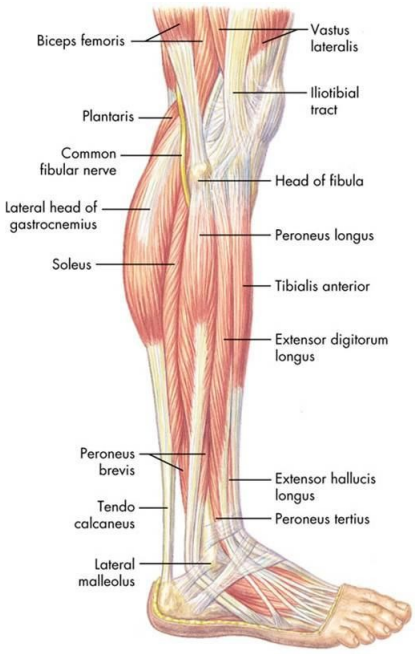

Figure 2-3 Ankle/foot muscles. (adapted from [7]).

2.2 Biomechanics of the Ankle/Foot Complex

Human lower limbs mechanisms, in particular the ankle-foot complex, are intricate and clever, allowing efficient and versatile movement. These mechanisms should be known to properly understand ankle mechanics and to inspire LEPE ankle designs that can approach human locomotion performance.

2.2.1 Walking

The normal walking gait cycle is divided into stance and swing periods. Stance is further divided into initial contact, loading response, mid stance, terminal stance, and pre-swing phases. Swing is also divided into initial swing, mid swing, and terminal swing phases (Figure 2-4). During walking, the body can be subdivided into two major units, the passenger unit and the locomotor unit. The passenger unit is composed of the head, arms, and trunk (HAT) and has negligible function in able-bodied level walking. The locomotor unit is composed of pelvis and two lower limbs and has four principal functions: stance stability, shock absorption, forward progression, and energy conservation [3]. Table 2-1 describes ankle function across the gait cycle.

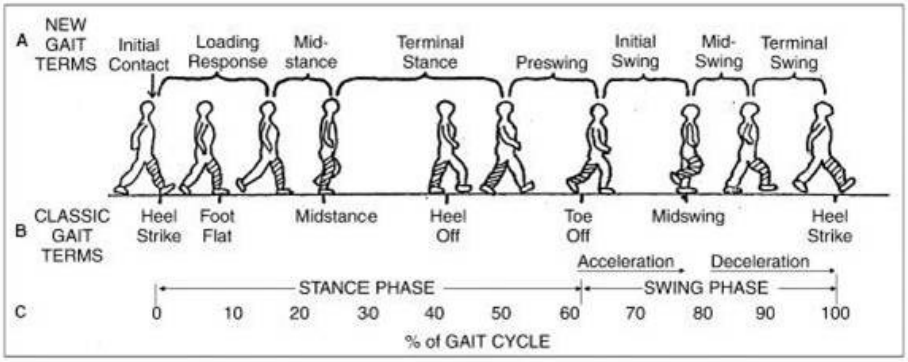

Figure 2-4 Gait phases (adapted from [7]).

Table 2-1 Ankle Function for all phases of the gait cycle [3]

Phase	% Gait Cycle	Movement	Function
Initial Contact	0-2%	Neutral ankle and toe dorsiflexion maintained	Ankle and toe dorsiflexors maintain neutral ankle position and incur tension in the plantar fascia to resist plantarflexion for deceleration of falling centre of mass (COM). The heel is rotated distally lengthening the limb and smoothing the COM trajectory.
Loading Response	2-12%	Controlled plantarflexion and subsequent dorsiflexion	COM deceleration is completed by controlled plantarflexion and then upward acceleration is aided by tendon recoil causing dorsiflexion motion. Plantarflexion minimizes knee flexion, hence necessary extension moment.
Mid Stance	12-31%	Eccentric dorsiflexion motion	The foot is maximally pronated, lowering the arch and hence absorbing body weight through plantar fascia tensioning. The Achilles tendon begins to stretch while calf muscles begin to increase activation eccentrically and finally isometrically.
Terminal Stance	31-50%	Continued dorsiflexion and heel rise	Plantar flexor torque decelerates forward COM fall. Achilles tendon and plantar fascia continue absorbing energy and stretching. Heel rise contributes to effective limb lengthening, minimizing COM fall. Calf muscles begin to decrease activity.
Pre-Swing	50-62%	Rapid Plantar Flexion	As load is transferred gradually to leading limb, the Achilles Tendon and plantar fascia begin to recoil, rapidly plantar flexing the ankle and producing a forward horizontal reaction force as well as contributing to the total vertical ground reaction force, effectively accelerating COM vertically and helping to advance swing limb.
Initial Swing	62-75%	Dorsiflexion motion	Tibialis anterior and extensor digitorum longus activated to dorsiflex toes and foot for clearance
Mid Swing	75-87%	Neutral	Tibialis anterior and extensor digitorum longus are relaxed
Terminal swing	87-100%	Foot and toe dorsiflexion	Tibialis anterior and extensor digitorum longus re-activated to prepare for controlled plantar flexion

2.2.1.1 Stability

The human body is naturally unstable because the HAT, which accounts for 70% of total body mass, rests on the locomotor unit support system. Stability can be modeled as an inverted pendulum with a point mass attached at the superior end representing the COM.

Due to the natural dynamics of some biped walker models, sagittal plane stability does not necessarily require any control for small perturbations since the gait cycle self-stabilizes at a certain

speed for a particular energy input. This has been demonstrated by passive dynamic walking robots with similar gait morphology to humans. The mechanism for gait pattern convergence to stability depends on energy losses during initial contact, implying that energy losses during initial contact promote stability. For larger perturbations, stability is gained by modulating foot placement of the swing limb and accelerating the swing limb forward to prevent forward falling. This rapid swing limb acceleration can be accomplished by ankle push-off modulation during pre-swing or hip flexor activity during initial swing. The faster the swing limb accelerates forward, the more robust the robotic walker stability [8]–[10].

These passive dynamic walker findings are corroborated in the field of biomechanics. Ankle muscles cannot be used to stop a forward fall during walking, with fall prevention achieved only by swing foot placement at initial contact [11]. Since 2D passive dynamic walkers with fixed ankles and rocker feet are stable, humans could maintain sagittal plane dynamic stability during walking without ankle muscles contributions, with the same movement conditions [12]. Moreover, studies using fixed ankle boots with rocker soles on humans did not increase metabolic energy consumption (i.e., additional metabolic energy was not needed to compensate for loss of ankle stability function if a rocker sole was included, for walking along a straight path) [13].

Medio-lateral stability following perturbations was studied using exoskeleton emulators, where many clever experiments were conducted to establish metabolic energy consumption and effectiveness of different medio-lateral stabilization strategies. Surprisingly, the most effective way to stabilize the body following ground height disturbances was ankle push-off modulation. On the other hand, following horizontal disturbances the most effective medio-lateral stabilization strategies were foot placement, followed by small inverter/everter ankle moments and ankle push-off work modulation [14]. Inversion/eversion ankle torque control was very effective for improving stability following ground height disturbances, although not as much as plantarflexion modulation, and moderately effective following lateral velocity disturbances. However, when inversion/eversion ankle torque control was added to step width modulation, stability (measured by metabolic energy expenditure) doubled. Inversion-eversion compliance could improve stability but not as well as torque control [15], [16].

For gait initiation and termination, COP location changes can accelerate the COM in the opposite direction. Changing the COP location is done in the sagittal plane by ankle dorsi and plantar flexors, whereas frontal plane COP changes are done by hip abductor/adductors by loading or unloading each limb [11], [17].

Greater toe-out angle corresponds to greater stability [3]. This is logical since the base of support is increased in the medio-lateral direction. This implies that LEPE ankle/foot designs with

natural toe-out feet would be beneficial. Toe out angle also leads to lower incidence of osteoarthritis since the GRF passes through the knee, thereby reducing knee abduction/adduction moments [18].

2.2.1.2 Energetically Efficient Forward Progression

During walking, the body COM moves along a sinusoidal path in the sagittal and transverse planes. Potential and kinetic energy are exchanged in equal proportions to maintain conservation of energy in the system, where potential energy is at its maximum during mid stance, when the COM is highest, and lowest during double support. Kinetic energy is at its highest when the COM is at its lowest position. However, there are energy losses since net metabolic energy increases above the metabolic baseline (energy expended during quiet standing) during level walking. The average net positive work produced at the lower limb joints during one gait cycle is 16 J [19].

Elastic energy storage in the human limbs is very important, specifically at the ankle-foot complex. Cavanagh and Komi [20] analyzed the ankle's energy efficient catapult mechanism during push-off by recording muscle fiber lengths and Achilles tendon length changes by ultrasound. Isometric plantar-flexor muscle contractions produced the most force, which is metabolically more efficient than concentric contraction, but produced negligible positive work. The plantar flexor muscles acted like clutches that maintain Achilles tendon tension, which passively stretches during most of stance phase until contralateral heel contact when the Achilles tendon quickly recoils from the stance limb being unloaded and releases the stored energy, thus producing high amplitude power impulse for push-off and swing limb momentum. Therefore, despite producing most of the positive work during gait, the ankle is mostly characterized by passive mechanics (i.e. the muscle can be replaced by clutches). The soleus muscle does shrink while force is being produced at the very end of stance phase, however the authors show that this happens after EMG activity has ceased meaning this positive work is also passive. However, there is a delay of up to 100ms occurring between EMG onset and muscle force generation [21].

This passive clutch-like mechanism was further validated using pneumatic ankle exoskeletons experiments. Ankle power efficiency (0.61) was much greater than typical muscle efficiency (0.1-0.25), implying an energy storing mechanism at the ankle foot complex [22]. This power efficiency is the mechanical work produced at the joint over the metabolic energy required for motion. Muscles require 4J to 10J of metabolic energy to produce 1 J of mechanical work, while the ankle produced approximately 2.44 J of mechanical work for each 4J of metabolic energy consumed.

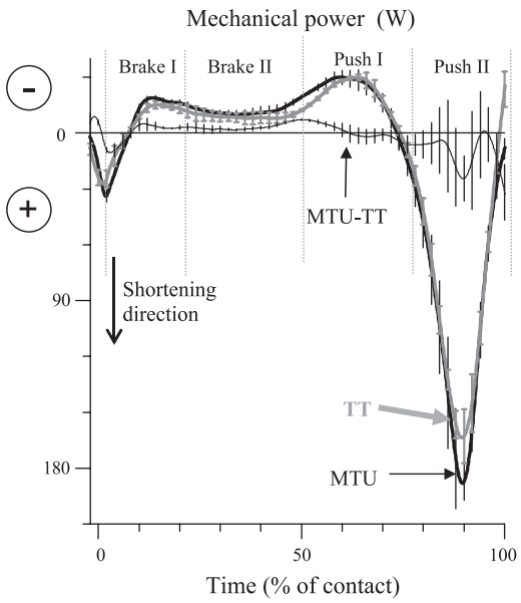

Figure 2-5 Energy efficient catapult mechanism. The TT curve represents power produced by Achilles Tendon whereas MTU-TT represents power at ankle joint due to muscle activity and MTU is the total power generated at the ankle (adapted from [20]).

While rocker soles minimize COM redirection work through limb length modulation [23] there is little research on the modeling or experimentation on the effect of limb length modulation in human walking. During initial contact, the ankle is in neutral position so that the heel becomes more inferior to the tibia, effectively increasing leg length. Heel rise in terminal stance increases effective leg length. Both effective length changes decrease COM excursion [3].

A modelling study showed that a passive windlass mechanism can improve walking efficiency by more than 15% across any walking speed [23]. Research investigating the energetic advantage of the windlass mechanism found that adding foot arch compliance can increase walking metabolic cost, therefore they concluded that energy savings from the windlass mechanism must come from reduced effective leg length during swing [24]. However, measuring windlass mechanism effects by proxy is problematic since the windlass mechanism is highly coupled to toe flexion, dorsiflexion [25], and plantar flexor activity (i.e. not limited to elastically deformable feet). Also, simply adding a degree of freedom at the metatarsophalangeal joint, even if only passive, increases both natural gait speed and energy efficiency [26], [27]. In work by Neptune [28], gastrocnemius, soleus, and proximal lower limb muscles were separated in terms of their contributions to vertical and horizontal trunk acceleration and work dedicated to swing limb advancement. As seen in Figure 2-6, both gastrocnemius and soleus provide the most significant contribution to COM vertical acceleration of any leg muscles during stance, while both muscles have differing effects on horizontal trunk acceleration during early stance. Gastrocnemius continues to decelerate forward

progression while soleus accelerates forward progression. Gastrocnemius contributed almost all its power to swing limb advancement during pre-swing while soleus continued accelerating the trunk forward. This result is interesting since, despite similar muscle location and activation pattern, the gastrocnemius is biarticulate and soleus is not, leading to functional differences.

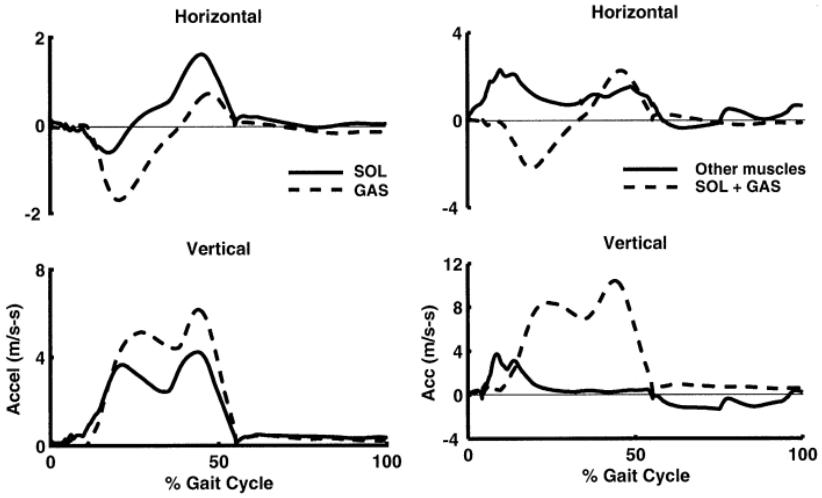

Figure 2-6 Contribution of gastrocnemius versus soleus to horizontal and vertical trunk acceleration (left), and gastrocnemius+soleus versus other muscles to trunk horizontal and vertical accelerations (right) (adapted from [28]).

2.2.1.3 Ankle/Foot Kinematics

The ankle's sagittal plane ROM consists of controlled plantarflexion at initial contact to maximum dorsiflexion during terminal stance, up to 15º, and rapid plantar flexing to a peak of up to 18º for a total ROM of approximately 33º (Figure 2-7). In the transverse plane, rotation has a maximum ROM of only 20º, where the ankle rotates externally relative to the tibia after initial contact and then gradually increases internal rotation until toe-off.

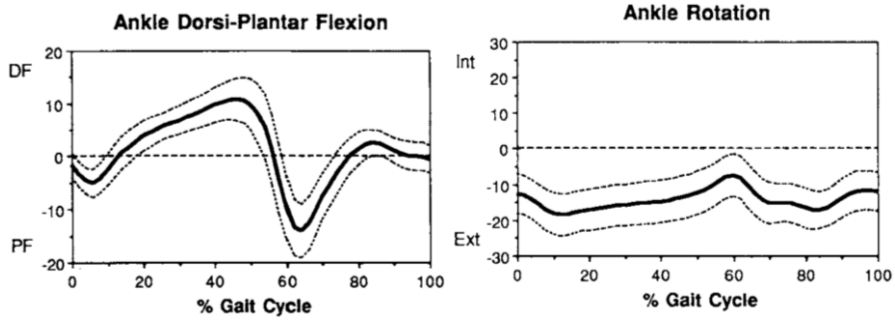

Figure 2-7 Ankle dorsiflexion and plantarflexion (left) and internal/external rotation during normal walking (right) (adapted from [29]).

For frontal plane kinematics, the ankle generally moves from passive inversion to eversion (peak eversion approx. 4º) during the first half of stance phase and transitions to inversion with a peak at the end of stance phase (approx. 7º) [30].

The toe is dorsiflexed during loading response, becomes neutral during foot flat, and is dorsiflexed during terminal stance and pre swing (Figure 2-8). The toe never plantar flexes during level walking and has a total ROM of approximately 25º.

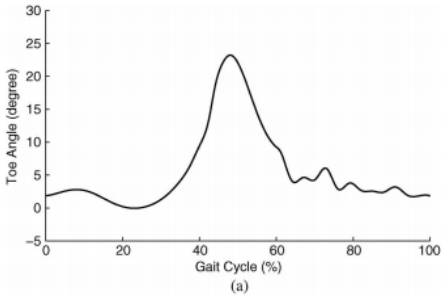

Figure 2-8 Toe angle during gait cycle (adapted from [31]).

2.2.1.4 Ankle/Foot Kinetics

Figure 2-9 shows ankle moments in each plane for one gait cycle. Torque demands are significantly greater in the sagittal plane (up to 1.5Nm/kg) compared to the other planes, although the dorsiflexion moment is quite small. External rotation moments reach a peak of about 0.1 Nm/kg. Frontal plane moments include a double eversion peak near the beginning and end of stance phase (global max of 0.1 Nm/kg) and a minimum inverter torque during late mid-stance of 0.05 Nm/kg.

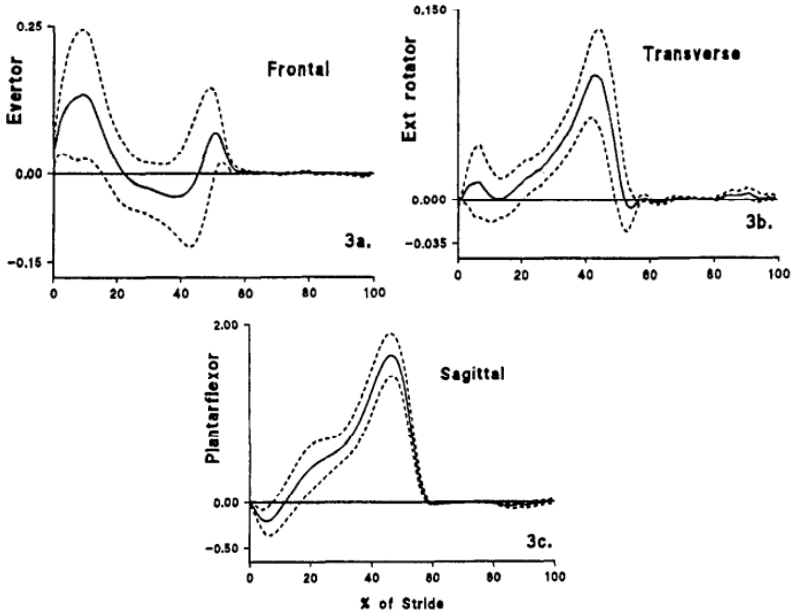

Figure 2-9 Ankle joint moments (Nm/kg) in frontal (left), transverse (middle), and sagittal (right) planes (adapted from [32]).

Ankle kinetics can be represented by moment-angle curves that show ankle stiffness throughout the gait cycle. If the curve forms a clockwise loop, the area enclosed by the curve is the net energy lost or absorbed by the joint, whereas the area enclosed by a counter-clockwise loop is the net energy produced by the joint during the entire gait cycle. For fast walking, the ankle moment-angle curve follows a counter-clockwise trajectory (energy generated). Normal walking is still counter clockwise but the area is smaller, meaning less energy was generated (Figure 2-10) [33]. The curve's direction is clockwise for slow walking, meaning net energy is absorbed at the ankle. Since current exoskeletons walk slowly, it should be possible to design an ankle that absorbs net energy (i.e., no need for active power generation) during walking with the same performance and function as a healthy biological ankle.

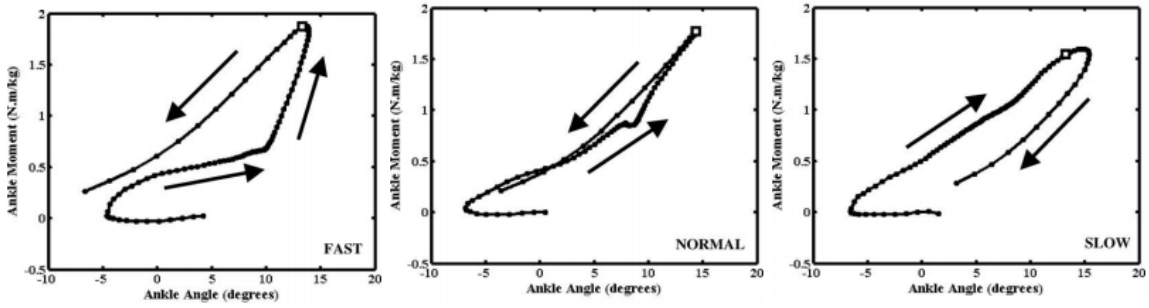

Figure 2-10 Ankle moment-angle curves fast (left), normal (middle), and slow (right) walking speeds (adapted from [33]).

Gait cycle power curves show peak energetic requirements of actuators (such as muscle-tendon units in humans or motor-spring units in robots). Ankle power in the transverse and frontal planes are negligible, with high variance [32]. However, controlled eccentric ankle eversion at initial contact and early loading response aids shock absorption [3]. Ankle power in the sagittal plane is substantial (Figure 2-11). Peak power occurs during pre-swing, increases with gait speed, and attains 3W/kg for normal walking and 2.3W/kg for slow walking.

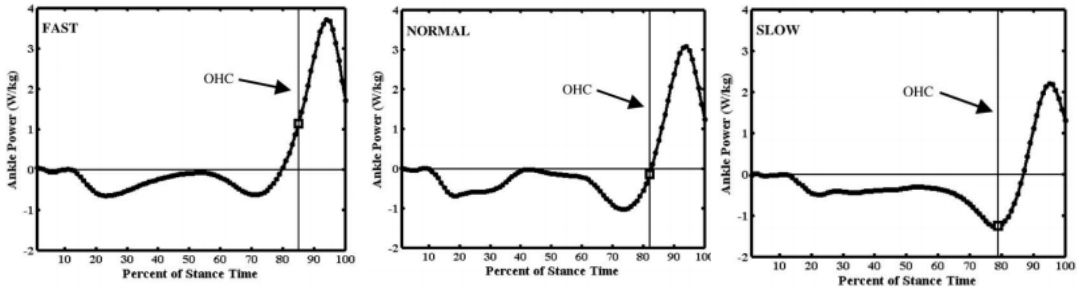

Figure 2-11 Ankle power at fast (left), normal (middle), and slow (right) walking speeds. OHC represents opposite limb heel strike (adapted from [33]).

2.2.1.5 Ankle Stiffness

Ankle quasi-stiffness can be measured from the slope of the ankle moment-angle curves. Linear rotational springs can model the ankle fairly well with high r^2 values for linear regressions [35]–[40]. Stiffness coefficients from linear regression slopes consistently range from 3 to 6 Nm/rad/kg, with coefficients increasing with walking speed. However other research has suggested the ankle stiffness is better described non-linearly, where stiffness increases with increasing dorsiflexion [35], [39]. Some studies suggested that the ankle moment-angle slope may not be equal to stiffness since the ankle is actuated by active muscles [40], [41]; however, others have shown that quasi-stiffness measured from ankle moment-angle curves is very close to the ankle's real stiffness [39], [40]. This is likely true because the ankle is dominated by passive mechanics even for normal walking speed. Furthermore, a study measuring true ankle impedance, by measuring the joint's response to known perturbations, determined that ankle impedance was mostly dominated by its stiffness and not viscous or inertial properties [39].

2.2.2 Four-Point Gait with Crutches

Most exoskeletons require people to use crutches for balance. The first approach for forearm crutch walking consists of moving both crutches simultaneously after each foot strike, while the second involves moving the right crutch after right foot strike and only swinging the left limb after the right crutch has contacted the ground, then repeating for the left side. When using forearm crutches, up to 50% body weight is supported by the arms [42]. Such extensive use can lead to upper limb pathologies and pain [43]–[47]. Minimizing upper limb load should lower an exoskeleton user's energetic expense, thus increase walking time before fatigue.

2.3 Walking Assistance Devices

This section reviews devices that assist in bipedal locomotion; specifically: exoskeletons, prostheses, orthoses, and biped robots.

2.3.1 Ankle Mechanisms in Commercial Exoskeletons

Five lower limb exoskeletons are commercially available: eLegs, ReWalk, Rex, Indego, and HAL (Figure 2-12). The focus of this section will be on ankle joint mechanisms.

eLegs from Ekso Bionics has revolute joints at the ankle whose axes are perpendicular to the sagittal plane (1 DOF). Passive torsional springs allow plantarflexion during early stance and dorsiflexion during mid to late stance. The springs return the foot to a neutral position to aid in foot

clearance. Average gait speed of SCI Ekso users was 0.14 m/s [53] although they claimed up to 0.89 m/s walking speed. Crutches are needed for balance and provide user-input for the control system.

eLegs (adapted from [48])

ReWalk (adapted from [49])

Indego (adapted from [50])

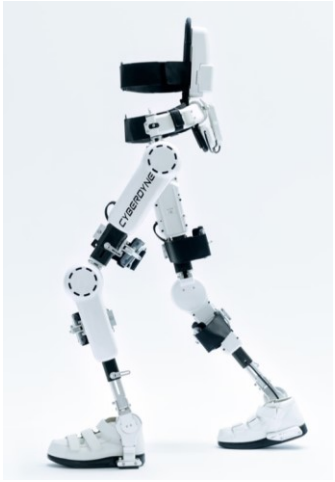

HAL (adapted from [51])

REX (adapted from [52])

Figure 2-12 Commercial exoskeletons.

ReWalk allows ankle rotation only in the sagittal plane (1 DOF). A unidirectional spring keeps the ankle dorsiflexed during swing phase. Since the spring is unidirectional, foot slap could occur. The bidirectional revolute joint is extremely light and compact despite containing a torsional spring. Crutches are needed for stability. Average gait speed of SCI ReWalk users was 0.28 m/s [53].

The Indego exoskeleton has no ankle joint. However the design is modular and the shank portion can be replaced with any ankle-foot orthosis design. This is advantageous since user specific

ankle-feet can be used. Typically, semi-rigid carbon-fibre AFO are used. Crutches are needed for stability. Average gait speed of SCI Indego users was 0.31 m/s [53].

Early versions of HAL exoskeletons used single DOF passive ankle joints with springs that aided in stability during stance phase and foot clearance during swing phase and did not provide ankle push off [54]. However, recent HAL iterations intended for users with paraplegia (HAL-5 LB type C) use powered ankle joints (1 DOF in sagittal plane). The powered ankle joint was used particularly for postural control [55]. For sit-to-stand, the ankle and hip actuators control plantar COP to maintain stability. An instrumented support bar aided users during sit-to-stand; however, reliance on the support bar was not reported. Although not specifically mentioned, it is believed the ankle joint uses the same transmission and motor configuration as the knee and hip joints, which consists of an electric motor and harmonic drive system.

Exceptionally, REX balances itself without SCI users having to use crutches. To ensure stability, REX has wide feet and five actuator DOFs per leg. Sagittal plane stability is controlled by ankle and hip actuators that control rotation in this plane. Frontal plane stability is controlled by ankle and hip actuators that control abduction and adduction at these two joints. Custom linear actuators are used but no further details are available. Although average gait speed was not found in the literature, the device moves very slowly to maintain postural balance.

Unfortunately, a trait these LEPE have in common is their slow speed and extensive need of crutches. In a systematic review of LEPE gait speed, Louie et al. [53] showed that the average speed achieved by SCI LEPE users was 0.26 m/s, well below the recommended 0.49 m/s needed for community ambulation [56]. These system limitations present a hurdle for the long-term success and adaptation for LEPE.

2.3.2 Academic Research Exoskeletons

Various LEPE and LEPE emulators have been designed and tested for research purposes, allowing quantitative analyses of different ankle mechanisms. Ideally, exoskeletons design have low power requirements to extend usage time. Exoskeletons that are capable of effortless faster gait speeds, compared to current models, are also desirable, but faster walking can require more power.

Many attempts have been made to design passive exoskeletons that reduce the metabolic cost of walking, some with limited success [57]. An MIT passive exoskeleton used electric power to engage clutches or modify knee damping, with dorsiflexion resisted by a very stiff unidirectional spring that absorbed energy during stance and released energy at push-off. A lower stiffness unidirectional spring maintained dorsiflexion during swing. Small eversion/inversion and internal/external rotation were permitted through a compliant carbon fiber plate attached to the boot.

Although the exoskeleton increased metabolic cost of walking, compared to no exoskeleton, metabolic cost improved with springs at the hip, knee and ankle, compared to the exoskeleton without springs. The metabolic cost increase was mostly due to the mechanism's weight. The authors stated that a clutch activated biarticulate knee-ankle spring could reduce metabolic cost [58], [59].

A passive ankle exoskeleton design reduced the metabolic cost of walking by using a cam activated clutch (dependent on joint angle) that would engage or disengage a parallel spring to produce a similar catapult mechanism to the human Achilles tendon during push off. The clutch engaged during stance and disengaged for swing [60]. The clutch mechanism was small and lightweight, contributing to exoskeleton energy efficiency (Figure 2-13).

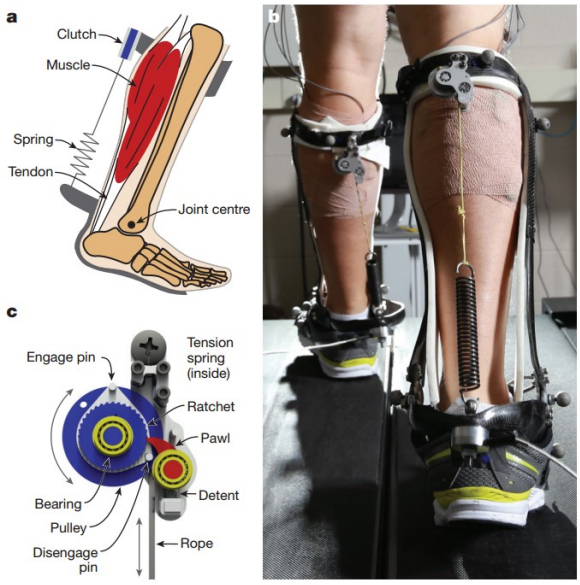

Figure 2-13 Clutch, catapult like mechanism of an ankle exoskeleton (adapted from [61]).

Various ankle exoskeleton designs, allowing only sagittal plane motion, were powered by pneumatic artificial muscles. Most of these designs also use EMG signals to proportionally control the force generated by the pneumatic muscles. Although these designs reduced metabolic cost of walking, had low weight/volume to force ratios, and had natural compliance they required a large volume of compressed gas or loud compressors that consumed excessive energy [62]–[64].

Herr et al. created a powered ankle exoskeleton that had the greatest reduction in walking metabolic cost, despite being relatively small and lightweight. This exoskeleton employed a catapult mechanism strategy but provided an additional 10 J of energy during each gait cycle and could produce up to 120 Nm of ankle moment, using fibreglass struts with a 30 cm moment arm about the ankle joint center. The actuator consisted of a winch mechanism, powered by a 200 W DC brushless motor. The entire transmission provided a 120:1 reduction ratio. The design also allowed transverse

and coronal plane motion [65]. Unfortunately, the moment arm length would make this design unacceptable by most people with disabilities.

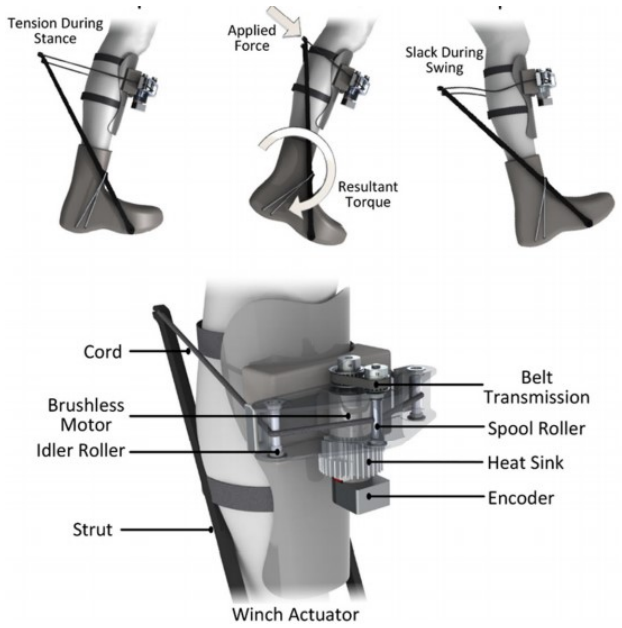

Figure 2-14 Powered ankle exoskeleton (adapted from [65]).

Elsewhere, a modeling study showed that adding a series spring to an electric actuator for an ankle exoskeleton could reduce peak power by 79% while a parallel spring could reduce ankle torque by 48% and rms power by 61% [66].

2.3.3 Prostheses

More research has been dedicated to ankle-foot designs in prosthetics compared to LEPE research, particularly in terms of maximizing efficiency and adaptability.

In prosthetics, energy efficiency has two principal focuses, lowering the user's metabolic energy consumption and minimizing prosthesis energy consumption to maximize battery life and thus prolong usage. Energy storing and returning (ESR) prosthetic feet were introduced to provide greater energy return (Figure 2-15). ESR feet generally have flexible keels that bend during stance, allowing dorsiflexion [67]. Although ESR feet reduced the metabolic cost of walking at speeds of 1.1 m/s, compared to older designs, these designs still produce less than 50% of biological ankle power and do not reduce amputees metabolic cost of walking to non-amputee levels [68].

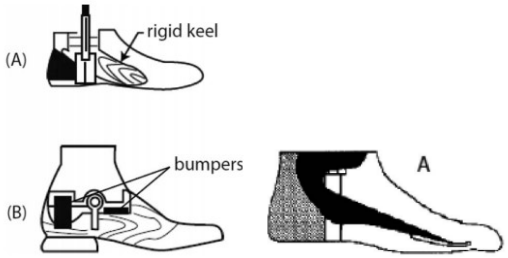

Figure 2-15 (left) Prosthetic feet: Cushioned heel (top), single axis of rotation with elastic wedges (bottom), Seattle-Foot ESR (right) (adapted from [67]).

Impedance control devices that use hydraulic dampers to control the virtual stiffness of leaf springs (e.g., Endolite Echelon foot, Figure 2-16) induce less compensatory mechanisms in intact joints and incur lower metabolic penalties during walking than ESR feet [69]. Subjectively, users stated their preference for these variable impedance prosthesis over ESR's, mentioning that they do not need to "climb over their prosthesis" while walking. The Echelon in particular has demonstrated smoother COP progression and lower GRF, which is attributed to the hydraulic damper more smoothly accepting body weight during loading response, leading to faster walking [70], [71].

The Echelon is a passive device that adapts to different walking speeds and terrain, including different slopes. The Echelon increases or decreases impedance with walking speed using hydraulic damping, where the level of damping force is proportional to the ankle joint's angular velocity. Plantarflexion and dorsiflexion resistances are both manually and independently configurable by modifying orifice size of one way valves. Controlled plantarflexion during loading response is believed to allow the knee to absorb energy and more effectively extend COM upward acceleration. The split toe foot permits inversion and eversion and an alternate version of the Echelon includes a torsional shock absorber that allows internal and external rotation for walking, smoother turning, and minimized motion between residual limb and prosthetic socket [72]–[74]. Torque absorber prosthetic designs allow transverse rotation above the sagittal plane revolute joint that may not be optimal energetically since, with normal toe out angles, the ankle joint is not in line with the plane of progression. In humans, transverse rotation of the foot/ankle complex relative to tibia occurs below the ankle joint. An interesting embodiment of the Echelon has the valve orifice area as a function of flexion angle, with smaller valve openings as the ankle rotates closer to maximum dorsiflexion or plantarflexion. This is similar to the biological ankle that passively increases its stiffness and dampening closer to the maximum ranges of motion [72], [75].

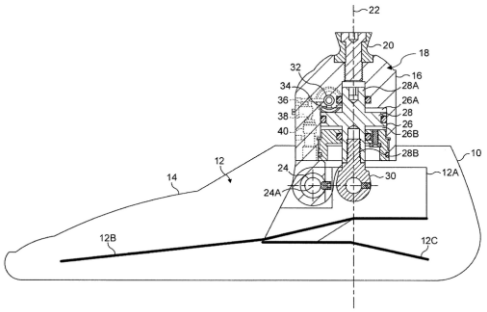

Figure 2-16 Endolite Echelon foot's hydraulic damper mechanism (28) (adapted from [72]).

Elan, a quasi-passive version of the Echelon, uses sensors to optimally control dorsiflexion and plantarflexion impedance by changing valve orifice diameters using a small DC stepper motor and transmission. Three operating modes include assist (low plantarflexion resistance but high dorsiflexion resistance), normal (equal resistance in plantar and dorsiflexion), and brake (opposite of assist). Assist is used mostly for walking and stair climbing, normal for standing, and brake for stair or incline descent. Assist and break allow or impede motion over the ankle. The Elan had better kinematics and improved metabolic consumption over conventional prostheses [76], [77].

Another quasi-passive foot design provided normal ankle peak power by storing energy during initial contact and loading response, and using clutch mechanisms to time power release during pre-swing (Figure 2-17). The device performed worse than conventional prostheses when tested on amputees. Since energy was stored during initial contact and not mid stance and terminal stance, as with the biological ankle, compensations at the hip and knee may have led to overall increased energy consumption. Knee co-contraction increased with this prosthesis, to provide stability, and the knee may have absorbed additional energy during terminal stance because the keel was too stiff [78], [79]. Altered loading response dynamics may have negated natural self-stabilizing features that use foot strike energy dissipation to achieve sagittal plane stabilization. Although this design introduced clever ways of storing energy, it was ultimately unsuccessful in part because the design was not biomimetic and thus had unintended negative energetic consequences.

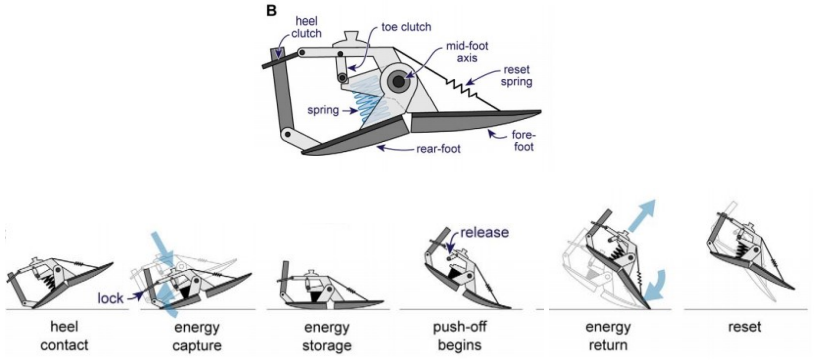

Figure 2-17 Quasi-passive energy storing device and action during stance phase (adapted from [78]).

The BiOM powered ankle-foot prostheses produced ankle plantarflexion power equal or superior to biological ankle power and successfully reduced metabolic energy consumption of amputees to non-amputee levels by incorporating a motor into the design. The design includes a typical flexible heel, keel with a split toe to allow inversion and eversion, and revolute ankle joint with a series elastic actuator and unidirectional parallel spring. The series spring reduced peak power and the parallel spring element reduced peak torque and further reduced electric motor power requirements. The prosthesis achieved a cost of transport (COT[1]) of only 0.06, consuming on average 30 J per gait cycle. Reduction ratio was achieved through a belt drive, ball screw transmission, and series leaf spring lever arm. The parallel spring is unidirectional to avoid plantarflexion resistance during pre-swing. The design weighed 2 kg, which is heavier than most prostheses but is approximately equal to amputated limb mass [80], [81]. One study observed limb asymmetries with BiOM because of a lack of gastrocnemius that helps advance the swing limb [68]. Multiple studies have demonstrated the effectiveness of using series elastic actuators to power plantarflexion however none have been as successful as the BiOM [82]–[84].

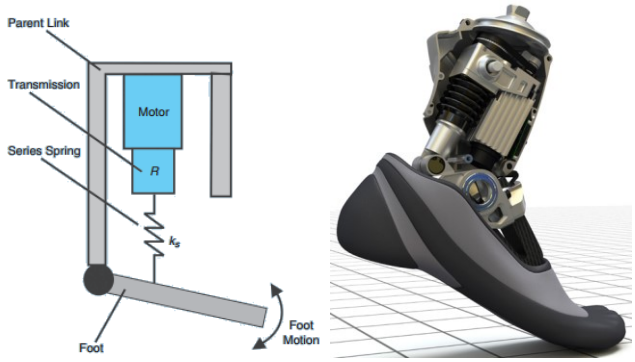

Figure 2-18 BiOM system [81] and BiOM with cover removed (adapted from [85]).

Studies using prosthesis emulators demonstrated that metabolic energy consumption decreased with increasing push off power, but with diminishing returns. These studies also showed that push off timing influences metabolic energy consumption, with optimal onset of push off occurring at or after opposite heel contact [86], [87].

2.3.4 Orthotics

Ankle-foot orthoses (AFOs) help stabilize people with weakened or spastic ankle muscles. For example, foot drop during swing phase could lead to tripping and falling and foot slap after initial

[1] Cost of transport is energy generated by electric power divided by (weight of subject times distance travelled)

contact could impede natural forward progression and create higher axial forces needed to rapidly decelerate the downward fall of the COM [88].

From kinetic and kinematic evaluation of a variable-impedance AFO (e.g., Figure 2-19), variable impedance had better performance than no or constant impedance for minimizing foot drop and increasing kinematic and kinetic similarity to able-bodied individuals [89].

Figure 2-19 MIT's Variable Impedance AFO (adapted from [90]).

In a study with able-bodied participants using a hip-knee-ankle-foot-orthosis (HKAFO), the kinetic and kinematic effects of locking or not locking the ankle were measured, and not locking the ankle led to reduced knee moments and reduced use of crutches [91]. From a modelling study, optimal stiffness for maximum energetic savings was not a function of most energy stored but a function of how and when the energy was released [92]. Another study demonstrated that when dorsiflexion was assisted during swing using a HKAFO, compensatory mechanisms and metabolic energy consumption were reduced [93]. Hinged AFO increase sit-to-stand speed compared to rigid AFO [94].

2.3.5 Biped Robots

2.3.5.1 Fully Actuated

As opposed to most powered biped robots in literature [95]–[97], the Spring Flamingo robot's (Figure 2-20) virtual model control considered non-linear dynamics of biped walking. Reduced parameters of the intuitive controller were iteratively modified to determine the most energy efficient combination. Two designs were presented, "point feet" and "ankle and flat foot". The robot with ankle and flat foot was faster and more energy efficient, could balance on one foot, did not have to walk with bent knees, and had smaller velocity fluctuations. Compliant ankles greatly reduced the torque requirements of an active actuator. The active actuator would only inject additional energy at

toe-off, thus not fighting the robot's natural dynamics. Quadratic springs whose stiffness was tuned in simulations, were used to achieve smooth center of pressure progression. The robot's ankle actuators were placed in the trunk and Bowden cables were used in conjunction with pulleys to transmit torque from the motors to the ankle to reduce leg moment of inertia [98]–[100].

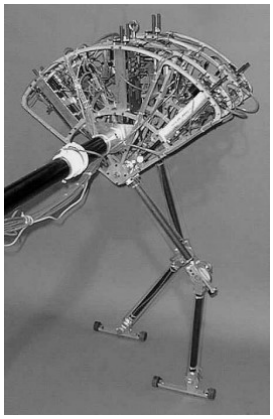

Figure 2-20 Spring Flamingo Robot (adapted from [99]).

2.3.5.2 Passive Dynamic Walkers

The interest in passive dynamic walkers is their energy efficiency and the use of simple controls, taking advantage of the natural dynamics of a system to produce energy efficient gait, as opposed to using feedback control to produce linear response thus fighting against the natural dynamics that will always result in less energy efficient systems [8].

In 1990, McGeer produced a biped machine with hips, knees, and curved feet that could walk relatively naturally in a stable manner down a modest incline, with gravity being its only energy input. This design cheated somewhat since the swing limb had to be shortened to clear the ground completely and used three limbs, two outside limbs whose movement was identical and a middle limb whose movement was reciprocal to the others [10]. However, other designs have only two limbs and sway laterally at each step to clear the swing limb. Balance is aided by arms that swing opposite from the lower limbs [101]. Designs using flat feet with compliant ankles worked almost as well as fixed ankles with curved feet, but slightly slower. The advantage of flat feet is improved standing balance and improved stability during walking [12], [102]. To walk on level ground, actuated joints were needed. One paper proposed virtual gravity fields to create moments at the hip and ankle that would create motion, as if the robot were on an incline whose angle is the control signal. Ankle moment control was a function of ankle angular position, which was interesting since this would simplify controls [103].

A dynamic walker with powered ankles and knees with clutches (Figure 2-21) was presented to walk on level ground [104]. Powered ankles produced the same power as the gravitational

potential from ramp walking. Active dorsiflexion during swing allowed foot clearance and spring energy storage. Spring energy was released by unlocking a clutch just after opposite heel contact. Despite modeling that determined push off before opposite heel contact was energetically preferred, with four times less collision losses, this approach put excessive mechanical strain on robot components and induced instability; therefore, push-off occurred just after opposite heel contact (similarly to humans). The simple controls included once-per-step timing to unlock the clutch at pre-swing.

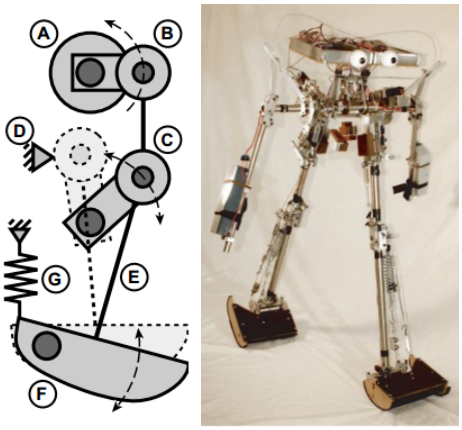

Figure 2-21 Powered ankle with motor (A), clutch (D) that maintained stretch in spring (G) during stance (left). Collins Dynamic Walker with powered push-off (right) (adapted from [104]).

This robot achieved a COT equal to humans (0.2) and a mechanical COT (total energy consumption replaced by mechanical work produced) similar to humans (0.055 compared to 0.05 in humans). Spring Flamingo achieved similar mechanical COT 0.07 but much worse total COT (2.8) since the series-elastic-actuators generated and absorbed a large amount of internal work. The ASIMO robot performed far worse than all mentioned in total COT (3.2) and mechanical COT (1.6), although ASIMO is capable of a range of movement activities. ASIMO natural dynamics were ignored and the robot was forced to follow particular angular trajectories. Since human muscles are quite inefficient (4J of metabolic energy converts to 1J of mechanical work on average), human walking and control takes full advantage of the body's natural dynamics and utilizes passive tendon/ligament energy storage in combination with eccentric muscle activity, with well-timed activations to produce low total and mechanical COT values [104]. Indeed, humans have displayed fractal gait properties indicating use of natural dynamics and chaotic behaviour [105]–[109].

2.4 Virtual Prototyping

Virtual prototyping can be a cost effective and time efficient way of prototyping different design ideas and estimating which will function best in the real world. Few studies have been

published on LEPE simulations and none have attempted to validate models. Two studies using ADAMS (MSC Software Corporation) and Matlab modelled and simulated control algorithms for stable LEPE walking, however a human model was not attached to the LEPE [110], [111]. Three other studies used ADAMS to simulate LEPE joint torques for various activities of daily living and evaluate joint controller performance [143]–[145]. These studies included an anthropoid model attached to the LEPE; however, the anthropoid models were highly simplified and attachments or interactions between LEPE and humanoid models were not described. Several interesting studies performed parametric or optimization simulations to determine ideal parameters for certain LEPE design components when performing activities of daily living [71], [146]–[150]; including, optimal series or parallel spring stiffnesses at lower limb joints, use of bi-articulate springs spanning knee and ankles etc. Ong et al. [119] included joint kinematics in OpenSim to determine optimal joint trajectories. These studies either used massless LEPE or used kinetics by normalizing joint torques to body weight and then multiplying joint torques by body weight plus the expected added weight of the LEPE, neglecting the altered mass distribution effects. Two studies looked at partial assist upper limb exoskeletons and recorded muscle activation reduction, one using AnyBody Modelling System (AMS) (AnyBody Technology) and the other using OpenSim [120], [121].

In a study modelling a real LEPE, Ferrati et al. [122] used OpenSim to compare joint moments between four conditions: no human attached, musculoskeletal model attached, LEPE allowing ankle motion but without human, and LEPE allowing ankle motion with musculoskeletal model attached. Although this study simulated “slow” walking velocities, the actual speed was not mentioned, making it hard to determine if the motion was representative of realistic LEPE slow walking. Furthermore, GRF were not taken into account, somewhat negating the usefulness of measuring joint moments. In a similar study, Zhu et al. [123] used LifeModeler (LifeModeler, Inc.) to obtain walking kinematics and ADAMS to model a real LEPE attached to an anthropoid model. This study measured joint alignment between human and LEPE and determined the required LEPE joint moments. However, this simulation did not consider GRF or use realistic LEPE walking speeds for spinal cord injured users. On the other hand, Cho et al. [124] used AMS to model a full-body powered exoskeleton (BLEEX for lower body, ABLE for upper limbs) that used predictive force plate modelling. The study compared the effect of strap locations on human joint loads for various activities of daily living. Able-bodied walking speeds were used.

Guan et al. [125] modelled a real unpowered lower extremity exoskeleton attached to a full body musculoskeletal model in AMS. Kinematics from a SCI user walking in the device, with the help of a walker, were used to drive motion of the combined system, while force plate data provided external force data to compute inverse dynamics. Walker GRF were not recorded so AMS reaction

forces were used to balance force equilibrium equations. This study optimized parameters for two springs located about the hip joint to reduce trunk and hip muscle activation. The model was validated by comparing measured EMG signals from trunk muscles to the model's predicted muscle activity. However, optimization's validity is unclear since adding springs to the design would alter gait kinematics, which in turn may lead to different muscle activations.

2.4.1 Predicting GRF

When simulating a combined LEPE-human model performing various activities, GRF prediction models are required if the motion is predicted or recorded from able-bodied people not wearing a LEPE.

Multiple GRF prediction techniques have been described and validated for activities of daily living, for humans not wearing a LEPE. For walking, GRF prediction during the double support phase is challenging since this an indeterminate case with multiple possible solutions. To solve this problem, one study used neural networks to predict GRF during double support, obtaining great accuracy [126]. However, neural networks require real GRF training data, which are not available if the motion was recorded without a LEPE. Studies also used spring-damper elements on the bottom of the foot to predict GRF; however, this strategy required forward dynamic simulation that can be computationally expensive [127], [128]. Another study used a rolling constraint in OpenSim to predict GRF; however, the model required centre of pressure and vertical GRF input from insole pressure sensors [129]. Multiple validation studies were conducted for the AMS contact model [130], [131]. This model uses nodes under the foot with small virtual muscle actuators and specified maximum strength. Each node contains five actuators, one for the vertical force and four for shear forces, with the shear force muscle's maximum strength being the normal force multiplied by a static-friction coefficient. The forces applied by the actuators are determined through the AMS muscle recruitment algorithm. The only inputs needed for this model are kinematics, which is convenient for LEPE studies using able-bodied motion. Another study presented improvements to this model that included velocity and distance between nodes and the ground to smooth discontinuities during heel-contact and toe off [132].

2.5 Summary of Findings

This review presented an overview of the anatomy and biomechanics of the ankle/foot complex as well as a review of the state of the art for ankle/foot mechanisms in exoskeletons, prostheses, orthoses, and biped robots. The ankle and foot were most responsible for stability and energy efficiency in human locomotion, although the biological ankle is undervalued for its shock

absorption function. To achieve the same energy efficient progression, sagittal plane stability, and shock absorption as the biological ankle during slow walking, an ankle foot design does not need to inject energy into the system but only absorb energy. Stability following different types of perturbations is achieved with the greatest efficiency by ankles that can modulate push-off power on demand, in both sagittal and frontal planes.

Passive dynamic walking robots have shown that using natural dynamics of biped machines instead of forcing linear behavior increases energy efficiency. Also, biped machines that walk using their natural dynamics display chaotic behavior at certain energy levels. This is advantageous since such systems are stable and can be very flexible. Thus, if an exoskeleton is designed that takes advantage of its natural dynamics it will display chaotic behavior that can also make it very flexible and stable. Designing a once-per-step control system for an exoskeleton that induces precise small perturbations can lead to very large changes in overall behavior. This allows a wide range of behaviors, each more or less suitable to a particular activity by inducing very small amplitude inputs.

These findings suggest that a LEPE ankle design that is capable of reducing crutch use by providing stable energy efficient progression should be biomimetic and utilize passive natural dynamics that are stable, fast, and efficient. To determine optimal design parameters for such a design, virtual prototyping techniques may be used to test the effects of biomimetic kinematics on LEPE ankle joint kinetics.

Chapter 3: Modelling and Simulation of a Lower Extremity Powered Exoskeleton

This chapter addresses the first and second objectives of the thesis. Two different ARKE LEPE and human musculoskeletal models were developed and implemented in the Anybody Modelling Software. The first model, called the biomimetic model, was driven by kinematics from 30 able-bodied participants walking at very slow speeds. The second model, called the SCI model, included crutches and was driven by 3D kinematics of spinal cord injured individuals using the ARKE. Both model's accuracy was validated by comparing predicted and measured GRF and COP.

The contents of this chapter were submitted to the IEEE Transactions on Neural System and Rehabilitation Engineering:

B. Fournier, E.D. Lemaire, A.J.J. Smith, and M. Doumit, "Modelling and simulation of a lower extremity powered exoskeleton," IEEE Transactions on Neural Systems and Rehabilitation Engineering, Oct. 2017, Submitted for publication.

3.1 Authors' contributions

BNF was involved with data collection, conception of study design, carrying out data analysis and interpretation, and drafting the manuscript. AJJS was involved with participant recruitment, data collection, conception of study design, and editing the manuscript. MD and EDL were involved with conception of study design and editing the manuscript. All authors read and approved the final manuscript.

3.2 Abstract

Lower extremity powered exoskeletons (LEPEs) allow people with spinal cord injury (SCI) to stand and walk. However, the majority of LEPEs walk slowly and users can become fatigued from overuse of forearm crutches, suggesting LEPE design can be enhanced. Virtual prototyping is a cost effective way of improving design; therefore, this research developed and validated two models that simulate walking with the Bionik Laboratories' ARKE exoskeleton attached to a human musculoskeletal model. The first model was driven by kinematic data from 30 able-bodied participants walking at realistic slow walking speeds (0.2-0.8 m/s) and accurately predicted ground reaction forces (GRF) for all speeds. The second model added upper limb crutches and was driven by 3D-marker data from five SCI participants walking with ARKE. Vertical GRF had the strongest correlations (>0.90) and mediolateral COP trajectory had the weakest (<0.35), for both models. These strong correlations between predicted and measured GRFs support use of these models for optimizing LEPE joint mechanics and improving LEPE design.

3.3 Introduction

Lower extremity powered exoskeletons (LEPE) allow people with spinal cord injury to stand, walk, and perform activities of daily living. Unfortunately, the majority of these assistive devices walk slowly and rely on forearm crutches for stability, thus may lead to premature fatigue and crutch overuse injuries [45], [53], [133]. Several approaches can improve understanding of exoskeleton biomimetic requirements and LEPE design. A typical engineering approach creates simple analytical models and makes good guesses to guide initial prototype design, and then iteratively builds new prototypes that improve the design. Others have built exoskeleton and prosthetic emulators that can be worn by a person and used to apply a range of joint moments and angular velocities, to simulate a wide range of possible design mechanics [134], [135]. Virtual prototyping (computer simulation) can also be used to measure optimal mechanical requirements, taking LEPE-human interactions into account, and can be more cost effective and time efficient.

Few studies have been published on LEPE simulations. Ferrati et al. [122] used OpenSim to compare joint moments with and without a real LEPE; however, this simulation did not take ground reaction forces (GRF) into account and used normal walking speed kinematics to drive the model. Slow LEPE walking (average 0.26 m/s [53]) differs from normal walking, substantially increasing time spent in double support, providing a "foot repositioning" style instead of a "push-off" walking style. Similarly, Zhu et al. [123] used LifeModeler (LifeModeler, Inc) and ADAMS (MSC Software Corporation) to model a real LEPE, measure joint alignment between human and LEPE, and calculate LEPE joint moments using forward dynamics simulation; however, this simulation also did

not take GRF into account or use realistic LEPE walking speeds for spinal cord injured (SCI) users. Cho et al. [124] used the AnyBody Modelling System (AMS) (AnyBody Technology) to present a full body powered exoskeleton model (BLEEX for lower body, ABLE for upper limbs) and compared the effect of straps on human joint torque and interaction forces between the human and the LEPE for different activities, including walking at normal speed. This simulation used inverse dynamics.

A number of other exoskeleton simulation studies focused on partial assist devices and biological muscle activity reduction [120], [121], [125]. Multiple studies used ADAMs simulated LEPEs to output joint torques and evaluate joint control performance for activities of daily living; however, these studies used highly simplified anthropoid models [112]–[114]. Two other studies used ADAMs to simulate LEPE walking however no humans were attached to the robot [110], [111]. Several studies simulated massless LEPEs to determine optimal design parameters, such as series or parallel spring stiffness at certain joints, for various activities of daily living [66], [115]–[119].

Although these studies shed light on LEPE requirements and optimized parameters for daily living activities, research is lacking for simulations that include a real LEPE attached to a full human musculoskeletal model, that walks at a realistic LEPE speed (very slow), with results validation. Simulations of LEPE-human systems driven by able-bodied kinematic data cannot use force plate data to perform inverse dynamics because the LEPE's added mass would result in different GRF. Therefore a predictive GRF model must be incorporated and validated.

Various techniques have been implemented to predict GRF. Two papers used multiple spring damper elements attached to the sole of the foot with good results; however, this technique required forward dynamic simulations that can be computationally expensive [127], [128]. Another technique used a neural network to predict GRF during double support phase of stance, with single support phase GRF determined from equations of motion; however, this technique required real force plate data to train the algorithm, which was not possible in this LEPE modeling research because the LEPE's added mass altered the GRF [126]. Hamner et al. [129] implemented a rolling constraint in OpenSim with excellent predictive ability but this method required centre of pressure (COP) location and vertical GRF data. A few studies implemented in AMS, validated and made iterative improvements to a GRF predictive model, that incorporated multiple actuators located under each foot into the AMS muscle recruitment optimization algorithm [130]–[132]. These models are particularly interesting since they predict GRF and COP location when the foot is in contact with the ground. The model from Jung et al. [132] was used in this research, with slight modifications.

This research presents two human-LEPE musculoskeletal models, implemented in AMS. The first is a biomimetic model driven by healthy slow walking kinematics. A successful model would

have high correlations and low errors between predicted and measured GRF and be validated using data from similar slow walking speeds encountered in LEPE use by people with paraplegia. A validated biomimetic LEPE model can be used in future research to enhance our understanding of exoskeleton biomechanical effects on the user and allow developers to explore design and control approaches to advance mobility technology. The second model (SCI model) incorporated crutches and was driven by kinematic data from paraplegic participants using a real LEPE. Predicted GRF accuracy would validate this model and further validate the biomimetic model since the measured force plate data from the second model were obtained from participants wearing the LEPE. A validated SCI model will be very helpful in measuring the effect of different gait strategies on upper limb loading and facilitate gait strategy recommendations that reduce user fatigue and extend LEPE time of use.

3.4 Model Development

A biomimetic model driven by abled-bodied kinematics was developed to replicate able-bodied motion and provide a means of obtaining mechanical requirements for LEPE joint designs that can perform these motions. A second model (SCI model) was driven by marker data collected from complete spinal cord injured users in a real LEPE. This model included crutches and was designed to replicate current LEPE capabilities. Motion and force plate data recorded from SCI participants walking in the LEPE were used to validate the GRF prediction model.

The combined human-LEPE was modelled with AMS [136]. Segment 3D marker data and external forces were input to a rigid multi-body segment system and AMS solved inverse dynamics equations to determine muscle and joint forces. An indeterminacy problem arose because the system was actuated by numerous redundant muscles; therefore, the AMS muscle recruitment optimization algorithm was implemented to determine muscle forces (Equation (1)),

$$G = \sum_i \left(\frac{f_i}{N_i}\right)^p \quad (1)$$

where G is the function to minimize, i the muscle identifier, f is the muscle force, N is the maximum muscle force and p is an exponent value (default, p= 3).

The Anybody GaitFullBody model was used for the human component. This model contained 37 bone segments and 69 degrees-of-freedom (DOF), including 3 at the hips, 1 at the knee, and 2 at the ankle (plantar/dorsiflexion, inversion/eversion). Lower extremity muscles were removed from the model to simulate paraplegia. Three dimensional movement analysis marker data provided kinematics for the human model.

3.4.1 LEPE Model

The LEPE model was developed using SolidWorks (Dassault Systemes SolidWorks Corporation) CAD files of the ARKE exoskeleton, provided by Bionik Laboratories (Toronto, Canada) (Figure 3-1), which included accurate inertial properties for all segments. This model had a mass of 33.6 kg and consisted of 13 segments with adjustable hip width, thigh length, and shank length. The model's hip joints allowed 3 DOF, knees allowed 1 DOF (flexion-extension), and ankles allowed 2 DOF (plantarflexion/dorsiflexion, inversion/eversion). The model allowed an additional two DOF at the hip and 1 at the ankle, which the ARKE did not have, to accommodate LEPE segment deformation and allow biomimetic motion.

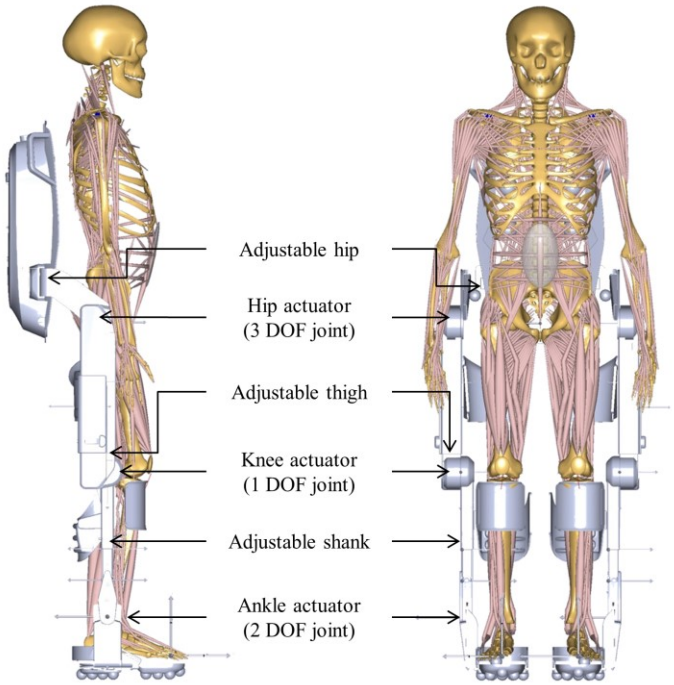

Figure 3-1 ARKE attached to GFB model

LEPE joint moments were provided by AnyGeneralMuscle objects with specified maximum strength. The forces generated by these virtual muscles were computed through the muscle recruitment optimization algorithm. AnyGeneralMuscle strengths were optimized to be as small as possible without overloading and to ensure that sagittal plane GRF pointed through or near LEPE joints. This naturally led to extensor virtual muscle strengths being much greater in magnitude than flexor virtual muscle strengths.

3.4.2 LEPE-Human Interaction

The LEPE was kinematically constrained to the human at the pelvis in all 6 DOF with human and LEPE hip joints aligned and at each foot in all 6 DOF, with LEPE and human ankle joints. The LEPE and human knee joints were aligned in the anterior-posterior axis. Constraints at the pelvis and knees were set to "soft", which allowed greater positional error of constraints, to permit some relative motion and to accommodate for a model that was kinematically over-constrained. Since the combined human-LEPE centre-of-mass (COM) was slightly posterior and inferior to the human-only COM, an ankle dorsiflexion correction was necessary to bring the COM forward to its original position (average correction was $2.21 \pm 0.38^{\circ}$). The ankle was chosen since this is the most efficient way to correct for small variations in COM position [137].

Interaction forces between the LEPE and the human were applied with AnyGeneralMuscles that acted in every DOF between LEPE foot and human foot, as well as in every DOF except axial force at the shanks, thighs, and pelvis. Muscle strength was determined by minimizing virtual muscle strength without overloading. Minimizing these forces was critical to ensure that the recruitment optimization algorithm did not make the muscles act as actuators, thereby unloading the ARKE joint actuators.

3.4.3 Ground Reaction Force Prediction Model

Since inertial properties of the combined system were different from the human only, human-only force plate data were replaced by Anybody's conditional contact force-plate model, based on [132] (Figure 3-2). Virtual muscle actuators located at nodes under the LEPE feet were included in the muscle force optimization algorithm and were active when these nodes were determined to be in contact with the ground. Five virtual muscles acted at each node: one in the vertical direction representing the normal force, two anterior-posterior, and two medio-lateral representing frictional forces. 170 nodes were placed under each foot, with a higher density near the toe region and nodes forming a curved pattern to better simulate rollover at terminal stance and obtain smoother and more biological GRF.

Speed and height criteria were used to determine when nodes contacted the ground contact cylinder. The speed criterion was defined from pilot test data using node velocity threshold below which the foot was not moving (2 x walking speed - 0.3). A height threshold was also used, below which the node was on the ground. The height threshold and maximum node muscle strength were modified for each participant to make GRF smoother and remove discontinuities while minimizing "hand-of-God" residual pelvis forces that were added to account for errors between GRF and inertial

properties. Average height threshold was 4.2 ± 0.5 cm and average maximum node muscle strength was 2.66 ± 0.96 BW.

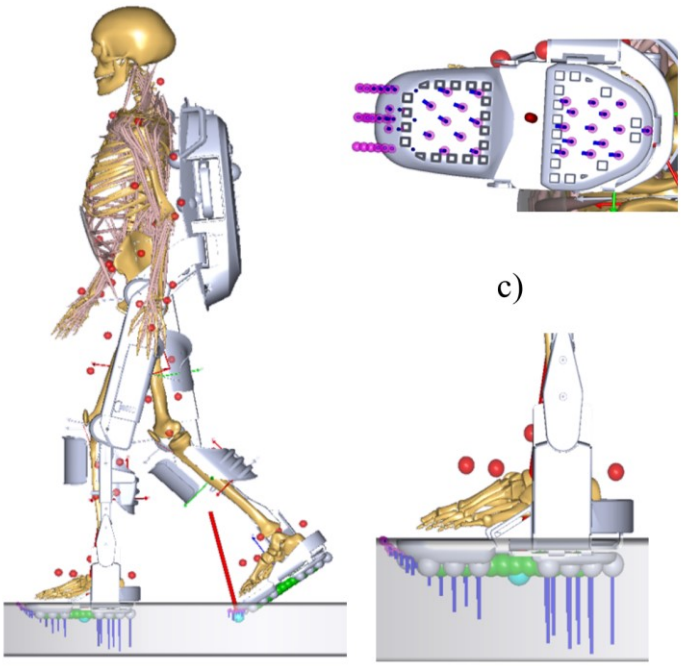

Figure 3-2 Full Human-LEPE model with ground contact cylinder (grey rectangular shape) and ground reaction force prediction model. Red dots are C3D marker positions. While walking, (a) trailing limb produced large GRF (red line) in part due to high toe node density and curved pattern, (b) left foot with normal forces at foot nodes (blue lines) representing virtual muscles, (c) plantar view of LEPE foot with ground reaction contact model nodes in purple.

If node velocity and height were above their respective thresholds, node muscle strength was set to zero. Otherwise these two values were used to modulate virtual muscle node strength using a cosine smoothing function. The closer these values were to their thresholds, the lower the virtual muscle node strength. This smoothed out discontinuities between swing and stance phase.

3.4.4 SCI Model

The SCI model was similar to the biomimetic model but with the following modifications (Figure 3-3). The eversion/inversion DOF was removed from the model since the real ARKE did not rotate in this plane. Ankle plantar-flexing muscles were removed since the real ARKE did not resist dorsiflexion. The extra hip DOFs remained to accommodate bending. Since a modified motion analysis marker setup placed markers directly on the LEPE, the human lower limbs were now driven

by LEPE lower limb motion and constraints between the human and LEPE model. The upper limb and torso kinematics were driven by markers placed on the human upper limbs and torso, as before.

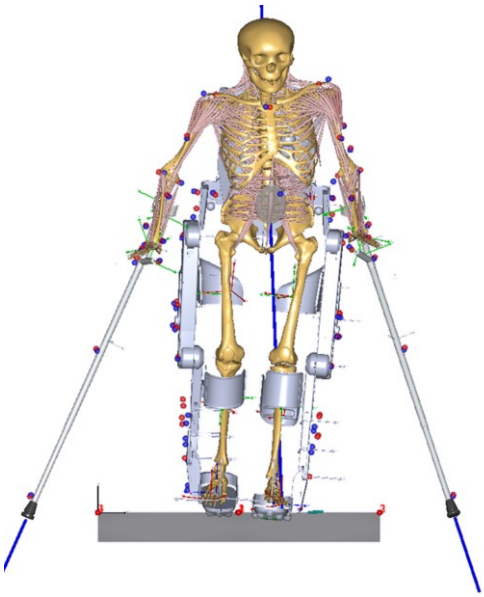

Figure 3-3 Human-LEPE SCI model with crutches and markers from SCI participants using ARKE.

Predictive ground reaction force model nodes near the edge of the feet were moved closer to the edge since ARKE users sometimes balanced on the edge of the foot to initiate contralateral limb swing. This created a larger possible base of support and COP closer to the foot's edge during large lateral leans.

3.4.5 Crutch Model

Forearm crutches were modeled in Solidworks and imported into AMS, with approximate inertial properties. Force data from real instrumented crutches were interpolated using a 4^{th} order spline curve and applied to the model at the distal end of the crutches, pointing in the crutch's axial direction. Normal forces between the crutch and human were applied using virtual muscles between the crutch cuff and human forearm. Forces between the crutch handle and human palm were applied in all DOF. Maximum virtual muscle strengths (AnyGeneralMuscle) were set to 50 N for linear kinematic measures or 50 Nm for rotational kinematic measures. Virtual muscle strength at the palm, in line with the crutch axis, was set to 500 N.

3.5 Validation

3.5.1 Participants

For biomimetic model development, a convenience sample of 32 able-bodied volunteers (height: 172.5±12.8cm, weight: 75.3±13.3kg, age: 30±10 years) were recruited from The Ottawa Hospital Rehabilitation Centre, Ottawa, ON, Canada and the community. For the SCI model, five people with complete spinal cord injury were recruited from the Ottawa Hospital Rehabilitation Centre (height: 179.1±7.4cm, weight: 74.5±3.1kg, age: 38±9.5 years). All participants gave informed consent and completed a consent form.

3.5.2 Able-bodied Biomechanical Data

Able-bodied participants were asked to walk at four slow speeds: 0.2 m/s, 0.4 m/s, 0.6 m/s, and 0.8 m/s in a CAREN-Extended system (6-DOF movable platform with dual force plate instrumented treadmill, 180 degree screen to project a virtual Park environment, Vicon motion capture system) [138]. Kinematic data were sampled at 100Hz with a full body marker set. Force plate data were sampled at 1000Hz. Slow speeds were used to accurately represent LEPE motion. Results for each participant were computed from 10 strides for each leg, for every walking speed. AMS simulations were batch processed where anthropometric parameter and kinematic trajectory optimization were followed by the inverse dynamics muscle recruitment optimization for each stride, leg, speed, and participant.

3.5.3 SCI Participant Biomechanical Data

SCI participants completed five, over-ground, self-paced walking trials (average speed: 0.14±m/s) over two force plates while wearing the ARKE exoskeleton. As required by the ARKE, participants initiated steps by leaning forward and laterally away from the swing leg. A 10-camera Vicon Motion Analysis System was used to collect kinematic data at 100Hz from a modified full body marker set, with lower limb markers placed on the ARKE. Force plate data were sampled at 1000Hz. Axial crutch forces were sampled at 50Hz using wireless instrumented crutches with strain gauges in a wheat-stone bridge configuration. Results were computed from one stance phase per foot for five trials. Force plate data were low-pass filtered using a second-order zero phase dual pass Butterworth filter with 15 Hz cut off frequency.

3.5.4 Data Analysis

Following [130] and [132], model performance was evaluated with Pearson-correlation ($r<0.35$, weak: $0.35<r<0.67$, moderate: $0.67<r<0.9$, high: $r>90$, very high) and root-mean-square error (RMSE) for GRF and COP trajectory. All GRF were normalized to body weight. COP was measured relative to the foot segment centre-of-gravity. Values were computed for each stance phase and then averaged. The last 5% of stance was excluded from COP analysis since toe-off timing estimation errors would disproportionately affect RMSE and correlation values.

Peak values from measured GRF and COP range were compared with peak values from predicted GRF and COP range, respectively, using two-tailed Wilcoxon signed rank tests. GRF peaks included X (medio-lateral, maximum and minimum), Y (anterior-posterior, maximum and minimum), and Z (vertical, 2 maximums and 1 minimum). COP range included X (medio-lateral) and Y (anterior-posterior).

3.6 Results

3.6.1 Biomimetic Model

Pearson correlations were significant for every speed and for all GRF and COP trajectories ($p<0.05$). When comparing speeds, GRF correlation coefficients were lowest for the slowest speed (Table 3-1). GRF correlation coefficients were highest in Z (very high) and lowest in X (moderate to high). RMSE were relatively small for Z GRF compared to X GRF and Y GRF, when compared to absolute GRF magnitudes (Figure 3-4). Peak analysis showed significant differences ($P>0.05$) between measured and predicted COP range for all speeds. For the faster speeds, predicted GRF Z was lower than measured GRF Z near terminal stance. For the slowest speed, predicted GRF Z was higher than measured GRF at loading response (Figure 3-4).

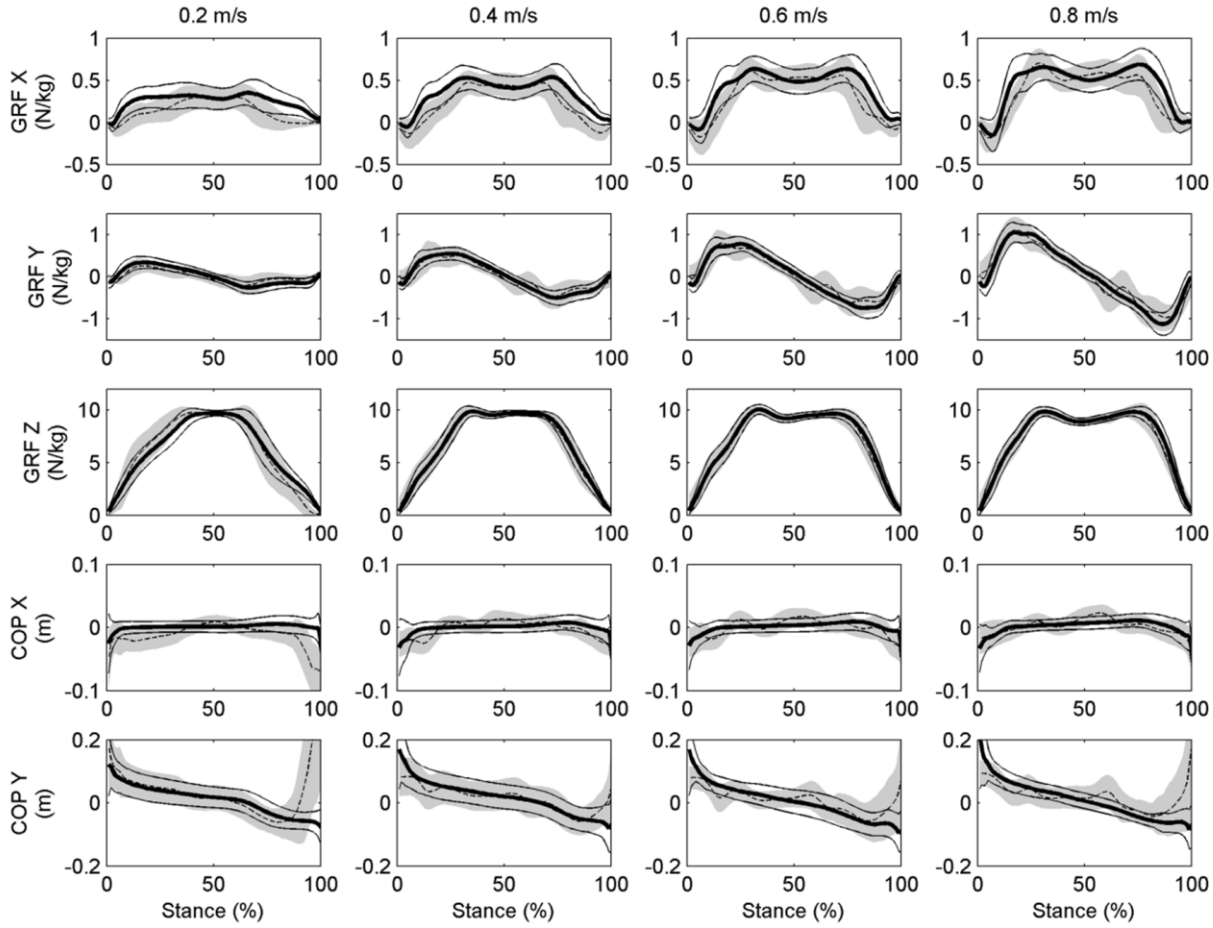

Figure 3-4 Biomimetic model predicted mass normalized GRF and COP trajectories (dashed line is mean, grey shaded area is mean±SD) and measured force plate GRF and COP trajectories (thick line is mean, thin lines are mean±SD) for four slow walking speeds.

Table 3-1 Biomimetic model average and standard deviation (in brackets) for Pearson correlation (r) and RMSE (N/kg) between predicted and measured ground reaction force (GRF) for different walking speeds (v) (m/s). Significant differences between min[(1)], first max[(2)], and second max[(3)] peaks are indicated.

	GRF X		**GRF Y**		**GRF Z**	
	r	***RMSE***	***R***	***RMSE***	***r***	***RMSE***
0.2	0.63 (0.19)[1,2]	0.17 (0.06)	0.70 (0.17)[1]	0.16 (0.03)	0.96 (0.03)[1,3]	1.07 (0.39)
0.4	0.79 (0.08)[1]	0.20 (0.05)	0.85 (0.09)[2]	0.22 (0.05)	0.98 (0.03)[1]	0.57 (0.27)
0.6	0.81 (0.07)[1]	0.20 (0.05)	0.88 (0.08)[1,2]	0.27 (0.07)	0.98 (0.02)[1,3]	0.59 (0.28)
0.8	0.81 (0.08)[1,2]	0.21 (0.06)	0.91 (0.06)[1,2]	0.31 (0.08)	0.98 (0.03)[1,3]	0.63 (0.26)

Correlation coefficients for COP X were low (<0.67) compared with COP Y (Table 3-2). Correlations for COP Y decreased with walking speed, while COP X correlation remained largely unchanged with walking speed, except for the slowest walking speed that produced the weakest correlations. COP Y was more posterior for predicted than measured outcomes near terminal stance for higher walking speeds.

Table 3-2 Biomimetic model average and standard deviation (in brackets) for Pearson correlation (r) and RMSE (cm) between predicted and measured COP for different speeds (v) (m/s)

v	COP X		COP Y	
	r	***RMSE***	***r***	***RMSE***
0.2	0.24 (0.33)	2.29 (0.95)	0.61 (0.41)	5.54 (3.84)
0.4	0.43 (0.24)	1.76 (0.60)	0.81 (0.14)	3.45 (1.50)
0.6	0.42 (0.26)	1.68 (0.43)	0.76 (0.18)	4.03 (3.29)
0.8	0.45 (0.29)	1.66 (0.45)	0.72 (0.21)	4.81 (3.75)

3.6.2 SCI Model

Pearson-correlations were significant for all GRF and COP trajectories ($p<0.05$) (Table 3-3 and Table 3-4). Correlations were stronger for vertical GRF and COP Y trajectory. While absolute RMSE were smallest for X and Y GRF and X COP trajectory, no significant differences were found between measured and predicted GRF peaks or COP range ($P>0.05$) except for medio-lateral GRF and vertical GRF peak at toe-off. Predicted GRF Z was higher than measured during terminal stance (Figure 3-5), while predicted COP Y was more posterior than measured during terminal stance (Figure 3-6).

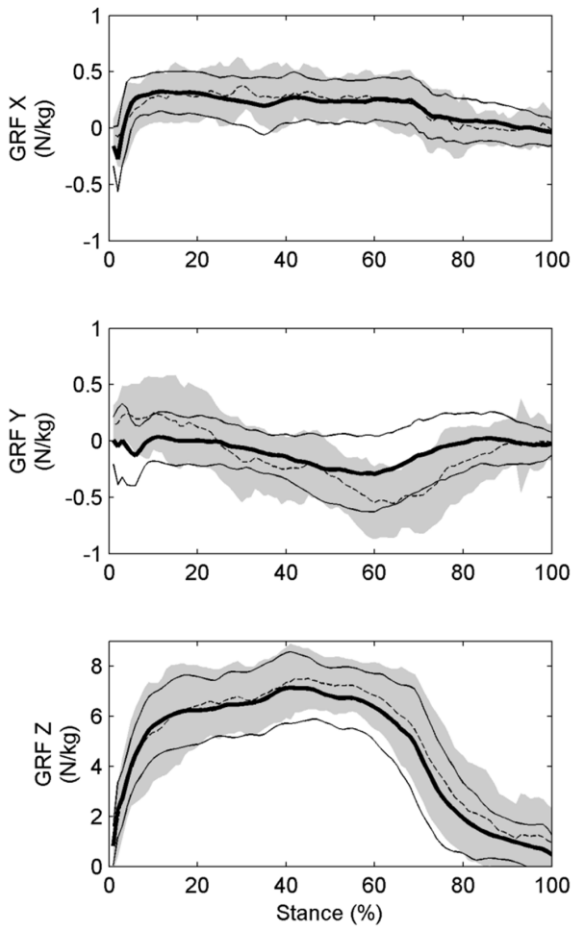

Figure 3-5 SCI model mass normalized predicted GRF (dashed line is mean, grey shaded area is mean±SD) and force plate GRF (thick line is mean, thin lines are mean±SD).

Table 3-3 SCI model average and standard deviation (in brackets) for Pearson correlation (r) and RMSE (n/kg) between measured and predicted GRF

GRF	r	RMSE
X	0.50 (0.21)	0.25 (0.07)
Y	0.50 (0.26)	0.34 (0.07)
Z	0.93 (0.16)	0.99 (0.51)

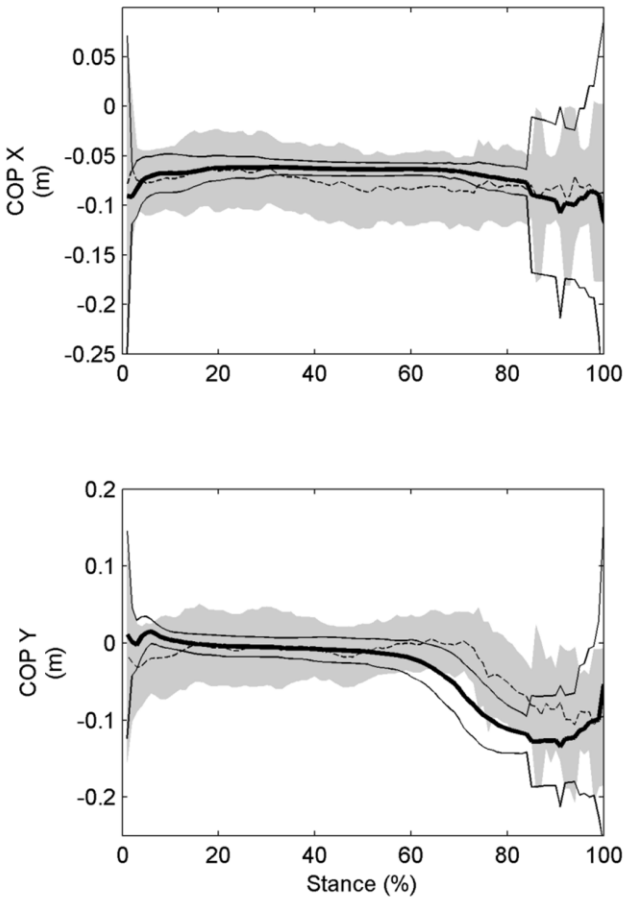

Figure 3-6 SCI model predicted COP trajectories (dashed line is mean, grey shaded area is mean±SD) and force plate measured COP trajectories (thick line is mean, thin lines are mean±SD).

Table 3-4 SCI model average and standard deviation (in brackets) Pearson correlation (r) and RMSE (cm) between measured and predicted COP trajectories

COP	R	RMSE
X	0.12 (0.35)	4.75 (3.03)
Y	0.46 (0.33)	6.21 (2.15)

3.7 Discussion

A total body simulation model that incorporates both the powered robotic exoskeleton and the person has great potential as a research tool to study powered exoskeleton effects on the body and as a design aid to evaluate interactions between the human and specific assistive device designs. This

study demonstrated the viability of such a model, developed using the AMS platform and ARKE exoskeleton, to provide sufficiently accurate and valid data to guide decision-making.

3.7.1 Biomimetic Model

As with a study validating the Anybody conditional contact model [132], the predicted vertical GRF had the strongest correlations to force plate data, followed by anterior-posterior GRF, and transverse GRF having the lowest correlation. This was likely due to an over-constrained knee model that did not include transverse rotation as well as lower signal-to-noise ratio for lower amplitude GRF X and Y [130].

The lower correlations for the slowest walking speed were likely due to longer double support times (DST). Longer DST leads to a greater potential for error since this is a statically indeterminate case that depends on Anybody's muscle recruitment algorithm to determine the share of GRF between both legs in contact with the ground.

In general, correlations between predicted GRF of users wearing the LEPE versus actual force plate GRF of participants without the LEPE were high, despite changes in inertial properties. In fact, correlations were comparable to those found in [130], [132] despite the slower walking speeds. This could perhaps be due to the modified foot node configuration improving results during DST. Interestingly, only small improvements in correlations were found with increasing walking speed beyond 0.2 m/s. In fact, correlations decreased slightly with increasing walking speed for GRF Z and COP Y.

Vertical GRF was underestimated at terminal stance for faster speeds and over estimated at loading response for slower speeds. This was due to the modified inertia when adding an exoskeleton or the GRF prediction model underestimating terminal stance Z GRF. Since the predicted loading limb Z GRF were not over estimated, and the residual pelvis forces were not strong enough to offset the difference in Z GRF, the cause of the lower predicted Z GRF was likely modified inertia.

The consistent sinusoidal pattern in predicted, but not real, GRF Y and COP Y at approximately 60% of stance phase (Figure 3-4) was most likely due to the modified inertia from adding the LEPE to the human model. This pattern's amplitude increased with walking speed, which would be expected since changes in inertia have greater effects at higher walking speeds and the pattern was present during single leg support, thus eliminating model DST errors as a potential cause. Specifically, this pattern may be due to increased swing limb inertia.

The higher predicted COP Y values near terminal stance could be due to early toe off prediction combined with a smoothing error that gradually moved the COP location back to the

global coordinate system after toe-off. COP range differences may also be due to these toe-off and heel-strike errors and the addition of the exoskeleton foot plate under the human foot.

Several limitations in the biomimetic model should be noted. A rigorous sensitivity analysis of predicted GRF model parameters and their effect on calculated GRF would be useful in further improving the model. Furthermore, healthy walking kinematics of individuals not wearing a LEPE were assumed to be optimal for individuals wearing a LEPE. The model partially mitigated this problem by correcting A-P COM position; however, inertial properties between an individual without a LEPE and an individual with a LEPE are different, which would lead to different natural dynamics and thus potentially different optimal walking kinematics. However, the high correlations found in this research suggest that inertial changes may be negligible, implying that biomimetic kinematics are appropriate for determining LEPE mechanics. Another model limitation may be the simplicity of the LEPE-human interaction. Model accuracy could be compared against a new model that includes more detailed interactions, such as a contact model that includes shear forces similar to Cho et al. [124].

3.7.2 SCI Model

Like the biomimetic model, the vertical GRF correlations were highest but the X and Y GRF correlations were only moderate, as opposed to high in the biomimetic model. This can partially be explained by the longer DST during slower speeds reducing model accuracy. The relatively low Y-GRF correlations may be due to the smaller magnitude and thus lower signal to noise ratio than the biomimetic model.

The relatively low X GRF correlation and differences in X GRF peaks can also partially be explained by low signal-to-noise ratio due to low magnitudes. This moderate correlation could also be due to force nodes not covering the foot's full surface and ARKE users balancing on the lateral edge of their feet when leaning to initiate a step. This would lead to the residual pelvis forces compensating for a lack of edge nodes needed to provide X-GRF at the foot. The lack of ARKE segment deformation modelling (i.e., segments modelled as rigid bodies) could have also contributed to these discrepancies. However, despite the lower correlations, the validation model's RMSE values were much lower than the biomimetic model [130].

COP correlations were moderate, with relatively low RMSE. Errors between measured and predicted COP trajectory were most likely due to low magnitudes, and thus small signal-to-noise ratio, as well as lack of edge nodes and lack of ARKE segment deformation modelling. The pulses near terminal stance in both COP X and Y (Figure 3-6) were due to instances of early predicted toe-off, where both measures suddenly move back to the global coordinate system origin.

For the first time, this SCI model can be confidently used to evaluate LEPE-human interaction forces, in particular upper extremity joint moments due to crutch use, or overuse. Simulated design modifications could be added to the model and optimized to reduce upper extremity joint loading.

3.8 Conclusion

Two human-LEPE models were developed using predictive GRF and then validated successfully against real force plate data. For the biomimetic model, correlations between measured and predicted values were high to very high for all GRF and moderate to high for all COP. For the SCI model, correlations were moderate to very high for GRF and weak to moderate for COP. Minimal significant differences were found between measured and predicted GRF peaks or COP range for the SCI model. The SCI model using kinematic data and force plate data from real SCI users in a real LEPE further validated the biomimetic model and can also measure human-LEPE interactions, such as upper limb joint loading from crutch use, a major limiting factor in LEPE time of use. The SCI model could be modified to include different LEPE joint designs and their effect on upper-limb joint loading could be measured. The validated biomimetic model can be used to measure optimal LEPE joint mechanics needed to reproduce able-bodied gait with minimal crutch use. These measured optimal LEPE joint mechanics can then be used as requirements for LEPE joint designs that can be implemented and optimized in the biomimetic model.

Future research will improve the model, including adding force nodes on the edges of the LEPE model's foot plate and validating LEPE model joint moments.

Chapter 4: Modelling and Characterization of Lower Extremity Powered Exoskeleton Ankle Mechanics for Very Slow Walking

This chapter addresses the third objective of the thesis. Biomimetic mechanical ankle requirements were determined for the ARKE LEPE for four realistic slow walking through simulation in the Anybody Modelling System.

The contents of this chapter were submitted to the Journal of NeuroEngineering and Rehabilitation:

B. Fournier, A.J J. Smith, M. Doumit, E.D. Lemaire "Modelling and Characterization of Lower Extremity Powered Exoskeleton Ankle Mechanics for Very Slow Walking. Journal of NeuroEngineering and Rehabilitation. Nov. 2017, Submitted for publication.

4.1 Authors' contributions

BNF was involved with data collection, conception of study design, carrying out data analysis and interpretation, and drafting the manuscript. AJJS was involved with participant recruitment, data collection, conception of study design, and editing the manuscript. MD and EDL were involved with conception of study design and editing the manuscript. All authors read and approved the final manuscript.

4.2 Abstract

Lower extremity powered exoskeletons (LEPE) allow people with spinal cord injury to stand, walk, and perform activities of daily living. However, current LEPE walk slowly and cannot be used for extended periods because users tire due to crutch requirements for balancing and weight transfer. The ankle contributes to speed and stability during able-bodied walking, but most LEPE lack a biomimetic ankle joint mechanism. This research investigated biomimetic ankle design requirements using a full 3D body model of a real LEPE (ARKE, Bionik Labs) attached to a human model, driven by 3D motion capture data of 29 able-bodied individuals walking at realistic LEPE slow walking speeds. Ankle range of motion, quasi-stiffness calculated from linear and quadratic regressions, work, peak moment, and peak power were compared between human and human+ARKE models, across four gait phases and four slow walking speeds. Ankle quasi-stiffness was significantly different across all gait phases and between human and human+ARKE models, and increased significantly with speed for controlled dorsiflexion and active plantarflexion phases. The human+ARKE model's ankle absorbed more total energy and produced negative net work, even for the fastest speed, compared to the human only model that produce positive net work for the fastest speed. Correlation coefficient (R^2) values for quadratic regressions were significantly greater than linear regressions while RMSE values were significantly lower for quadratic versus linear regressions ($p<0.05$). These results suggest that passive variable stiffness ankles incorporating quadratic elastic spring elements could achieve biomimetic ankle function for LEPE.

4.3 Introduction

People with spinal cord injury (SCI) are now able to stand, walk, and perform activities of daily living with the use of a lower extremity powered exoskeleton (LEPE). Although LEPE allow individuals with SCI to regain independence and offer many health benefits[139]–[143], these devices walk slowly and cause user fatigue when forearm crutches are overused, reducing possible time of use [45], [53], [144]. A common limitation of most LEPE is the lack of a biomimetic ankle joint mechanism. Whereas healthy human ankles have highly variable and non-linear mechanical impedance, depending on gait cycle, speed, and mode, among other parameters, most LEPE ankle designs provide constant limited support. This support can consist of a simple hinge with dorsiflexion biased spring for foot clearance and a mechanical hard stop limiting maximum dorsiflexion and plantarflexion, or a standard semi-rigid ankle foot orthosis. In lower limb prosthetics, variable impedance ankle designs enhance symmetrical gait between amputated and intact limbs, compared to constant stiffness designs, reducing intact limb overcompensation [77],

[79], [145], [146]. Since biped locomotion is typically more efficient with non-linear ankle stiffness [98]–[100], this factor should be considered for LEPE design.

The biological ankle is critical for energy efficient forward progression. During stance for able-bodied walking, the ankle contributes 60% of the positive work from the sum of ankle, knee, and hip [22]. The soleus and gastrocnemius muscles act on the ankle joint and are most responsible of all leg muscles for total body accelerations during walking [28]. Despite being most responsible for center of mass (COM) control, the ankle is mostly characterized by passive mechanics during normal and slow walking speeds [147]–[149]. With an adequate biomimetic ankle, a biped walker would have appropriate momentum control and be more efficient. Furthermore, orthotic ankle designs inspired by biological ankles have demonstrated the ability not only to reduce ankle joint muscle activity but also unload knee and hip joints during walking [150]. Given the vital role of the ankle for fast, energy efficient walking, and stability, applying a biomimetic ankle design to LEPE should enhance exoskeleton stability and walking speed, thus reducing user fatigue. This is especially true for LEPE that require leaning forward and to the side to initiate a step. Without an ankle capable of substantial dorsiflexion resistance, leaning forward induces added strain on the user's arms from weight shifting and preventing them from falling forward. With respect to side-to-side weight shifting, the most effective way to balance laterally while walking is to modulate ankle push-off power [151]. On the other hand, LEPE walking speed will be limited if the ankle is too stiff in early stance phase since this would impede forward momentum. This contradiction further emphasizes the importance of a variable resistance ankle.

To inspire prosthetic and orthotic design, many studies have investigated biological ankle walking mechanics. In particular, studies have estimated ankle stiffness by measuring the slope of ankle angle-moment curves, finding that linear torsional spring components model the biological ankle reasonably well during walking [33]–[38]. Although the ankle angle-moment curve slope is not a true measure of an active joint's stiffness, this quasi-stiffness measurement is very close to the ankle's real stiffness [39], [40] because the ankle is dominated by passive mechanics. Rouse et al. also determined that ankle impedance is mostly dominated by its stiffness and not viscous or inertial parameters [39]. However, none of these ankle mechanics studies are adequate for realistic LEPE slow walking speeds (average 0.26 m/s [53]).

Despite the increased interest and research into LEPE, research is lacking on characterization of biomimetic LEPE ankle designs. Ferrati et al. [152] compared joint moments with and without a real LEPE using OpenSim while Zhu et al. [123] used LifeModeler (LifeModeler Inc); however, these simulations did not use ground reaction forces (GRF). Two studies used ADAMS (MSC Software Corporation) simulation software, in conjunction with OpenSim and LifeModeler, to attach

exoskeleton CAD designs to human models performing healthy normal walking and sit-to-stand to determine necessary joint torques [112], [123]. Additional studies were designed to optimize certain LEPE joint design parameters such as parallel and series spring stiffness, for various activities; however, LEPE were assumed to be massless [66], [115]–[119]. Although these studies established possible biomimetic joint requirements for certain daily living activities, no research has determined biomimetic ankle design requirements for LEPE using validated models or simulations of a real LEPE performing realistic walking at very slow speeds.

This research presents a description of biomimetic mechanical ankle requirements for a LEPE using a human-LEPE musculoskeletal model driven by healthy slow walking kinematics. The rationale for mimicking biological motion for LEPE control includes the fact that healthy gait does not require crutches; thus, implementing biomimetic joint mechanics should reduce crutch use. Secondly, human walking is very energy efficient, especially compared to biped robots [104]. We expected to find that a biomimetic LEPE ankle should be passive and capable of variable non-linear stiffness. Results will inform recommendations for an improved LEPE ankle that will increase LEPE speed and stability, thus reducing crutch overuse and increasing time of use.

4.4 Methods

4.4.1 Participants

A convenience sample of 29 able-bodied volunteers (height: 172.5±12.8cm, weight: 75.3±13.3kg, age: 30±10 years) were recruited from The Ottawa Hospital Rehabilitation Centre and the community. All participants provided informed consent and signed a consent form (Ottawa Health Science Network Research Ethics Board, 20150852-01H). Participants walked at four slow speeds: 0.2 m/s, 0.4 m/s, 0.6 m/s, and 0.8 m/s on a CAREN-Extended system (6-DOF movable platform with dual force plate instrumented treadmill, 180 degree screen, Vicon motion capture system [138]). Full body kinematic data were sampled at 100Hz from a full body marker set. Force plate data were sampled at 1000Hz. Outcome measures were computed from 10 level walking strides, from each leg, for all speeds and normalized to body weight.

4.4.2 Model

This study implemented a validated combined human-LEPE model [153] with the Anybody musculoskeletal software (AMS, Anybody Technologies [136]). The default AMS GaitFullBody model was used for the human component, which had 69 degrees-of-freedom (3 at hip, 1 at knee, 2 at

ankle). To simulate paraplegia, muscles were removed from the model's lower extremities. 3D movement analysis marker data provided kinematics for the human model.

The LEPE model was developed from SolidWorks (Dassault Systèmes SolidWorks Corporation) assembly files of the ARKE LEPE (Bionik Laboratories) (Figure 4-1). The LEPE model had a mass of 33.6 kg, hip joints allowed 3 DOF, knees allowed 1 DOF, and ankles allowed 2 DOF. Virtual muscles provided LEPE joint actuation.

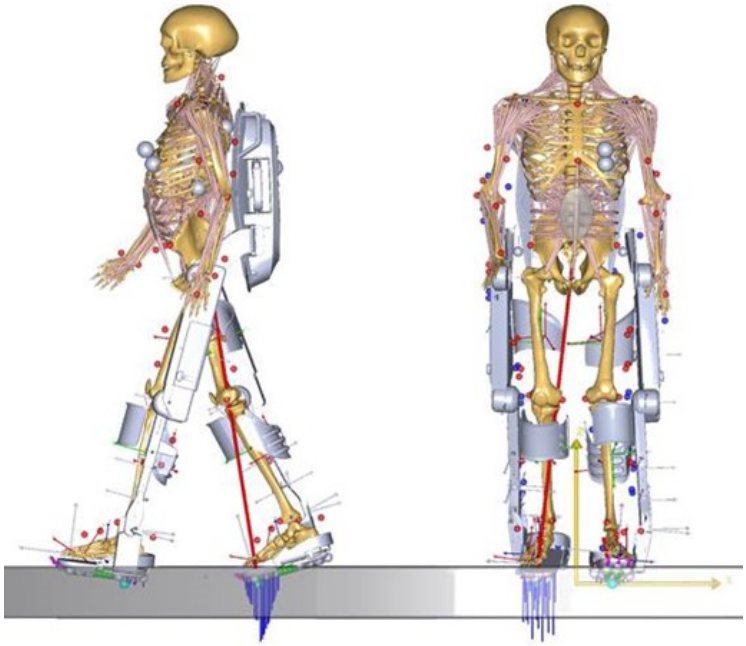

Figure 4-1 Full Human-LEPE model walking, with ground contact cylinder (grey rectangular shape under feet) and ground reaction force prediction model. Trailing limb produced larger GRF (red line for resultant GRF, blues lines for virtual node muscles).

The LEPE and human were kinematically constrained together in all DOF at the hip and feet. An additional constraint was added to ensure LEPE and human knee joints were aligned in the anterior-posterior axis. An ankle dorsiflexion correction was also necessary to bring the total body centre-of-mass (COM) forward to its original position (average correction was $2.21 \pm 0.38^{\circ}$) because the LEPE-human COM was slightly posterior and inferior to the human-only COM. Inertial properties of the combined system were different from the human only; therefore, force plate data were replaced by a predictive GRF model that was modified slightly from [132], incorporating muscle-like actuators that provided normal and frictional force vectors located at node contact points under the LEPE feet. These muscle-like actuator forces were computed through Anybody's muscle recruitment optimization algorithm.

4.4.3 Data Analysis

For passive ankle dynamics, and to a small extent active dynamics, ankle quasi-stiffness (Equation 1) is similar to ankle stiffness,

$$k = \frac{dM}{d\theta} \tag{1}$$

where k is quasi-stiffness, M is ankle moment, and θ is ankle angle. Since slow walking is characterized by passive ankle dynamics (energy absorption), biomimetic ankle mechanics were described by quasi-stiffness [39], [40]. Following [33], [35], walking was split into four phases: controlled plantar flexion (CPF) from the beginning of stance to first local plantarflexion maximum, controlled dorsiflexion (CDF) from first plantar flexion maximum to dorsiflexion maximum, powered plantar flexion (PPF) from maximum dorsiflexion to zero GRF Z, and swing (S) (Figure 4-2 and Figure 4-3).

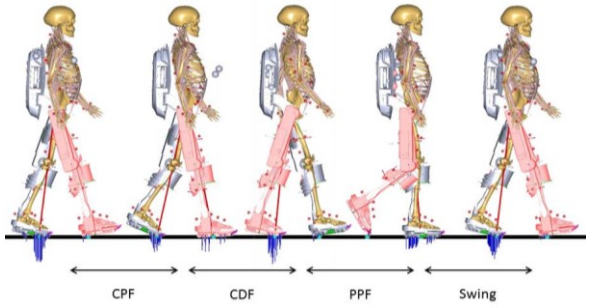

Figure 4-2 Gait divided into phases: CPF (controlled plantar flexion), CDF (controlled dorsiflexion), PPF (powered plantar flexion), and swing.

Quasi-stiffness was computed for each phase, each speed, and with or without ARKE by linear and quadratic regression. Ankle work was computed for CDF and PPF phases and total stance. Work was compared between with and without ARKE for each phase and walking speed. Quality of regression fit was measured using R^2 and root-mean-squared-error (RMSE) to determine whether linear or quadratic springs would be better suited to reproduce biomimetic ankle mechanics. Peak ankle dorsiflexion, plantarflexion, moment, and power were also computed for all conditions.

Statistical differences in ankle quasi-stiffness regression coefficients were assessed using three-way ANOVA tests with predictors being whether ARKE was worn, gait speed, and gait phase. Differences in R^2 and RMSE were analyzed using two-way ANOVA with factors being linear versus quadratic regressions and gait speed. Differences in ankle work were analyzed using two-way ANOVA with gait speed and with or without ARKE as predictors. Differences in ankle peak dorsiflexion, plantarflexion, moment, and power were analyzed using two-way ANOVA with predictors being with or without ARKE and gait speed. Post hoc analyses were computed using

Tukey's honest significant difference procedure ($p<0.05$). Statistical analyses were computed using the statistics and machine learning toolbox from Matlab v2016.

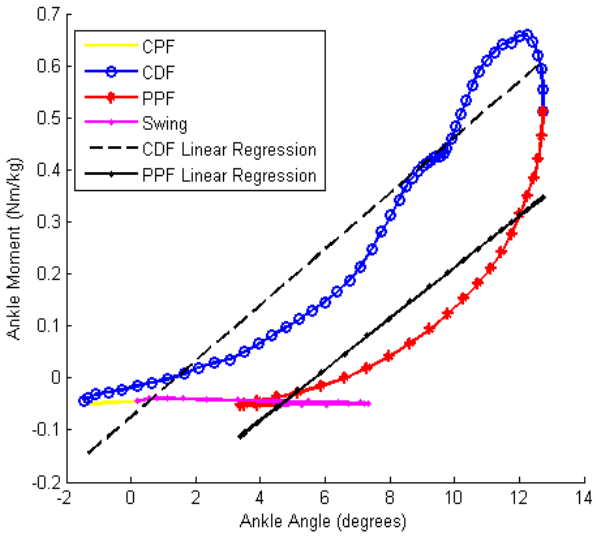

Figure 4-3 Ensemble average LEPE ankle moment-dorsiflexion angle curve split into four gait phases (0.2 m/s). The dashed and dotted lines represent examples of linear regressions for controlled dorsiflexion and powered plantar flexion, respectively.

4.5 Results

Mean ankle quasi-stiffness estimated by linear regression varied significantly between gait phases (Table 4-1). Quasi-stiffness between with and without ARKE was significantly different across all conditions and quasi-stiffness was significantly different between all speeds except between 0.6 m/s and 0.8 m/s. Without-ARKE, quasi-stiffness within phases, except swing, were significantly different, with quasi-stiffness almost always increasing with speed. With-ARKE, quasi-stiffness was not significantly different between phases, except during PPF where quasi-stiffness at 0.2 m/s was significantly less than quasi-stiffness at 0.4 m/s.

Without-ARKE, the lowest ankle quasi-stiffness occurred during swing, with larger stiffnesses progressing from CPF to PPF, and CDF. With-ARKE, lowest ankle quasi-stiffness occurred during swing, increasing between CPF, CDF, and PPF. Ankle quasi-stiffness without-ARKE was lower than with-ARKE during PPF but greater during CDF (Figure 4-4).

Table 4-1 Mean linear ankle quasi-stiffness (Nm/rad) for walking speeds, gait phases, and with or without ARKE exoskeleton. Standard deviation in brackets.

Speed (m/s)	K_{CPF}		K_{CDF}		K_{PPF}		K_S	
	ARKE	***No ARKE***	***ARKE***	***No ARKE***	***ARKE***	***No ARKE***	***ARKE***	***No ARKE***
0.2	0.31 (2.33)	-0.02 (3.29)	2.79 (1.43)	2.52 (1.17)	2.36 (3.46)	2.77 (1.97)	-0.03 (0.06)	-0.01 (0.08)
0.4	0.19 (0.99)	0.64 (1.61)	2.66 (1.18)	2.94 (1.05)	3.77 (2.20)	2.89 (1.05)	-0.03 (0.08)	-0.02 (0.06)
0.6	0.29 (1.20)	1.05 (6.21)	2.97 (1.18)	3.27 (1.09)	4.49 (2.25)	3.22 (0.94)	0.02 (0.19)	-0.01 (0.19)
0.8	0.37 (1.25)	1.13 (0.78)	3.23 (0.99)	3.67 (0.89)	4.47 (1.31)	3.31 (0.74)	0.06 (0.13)	-0.00 (0.06)

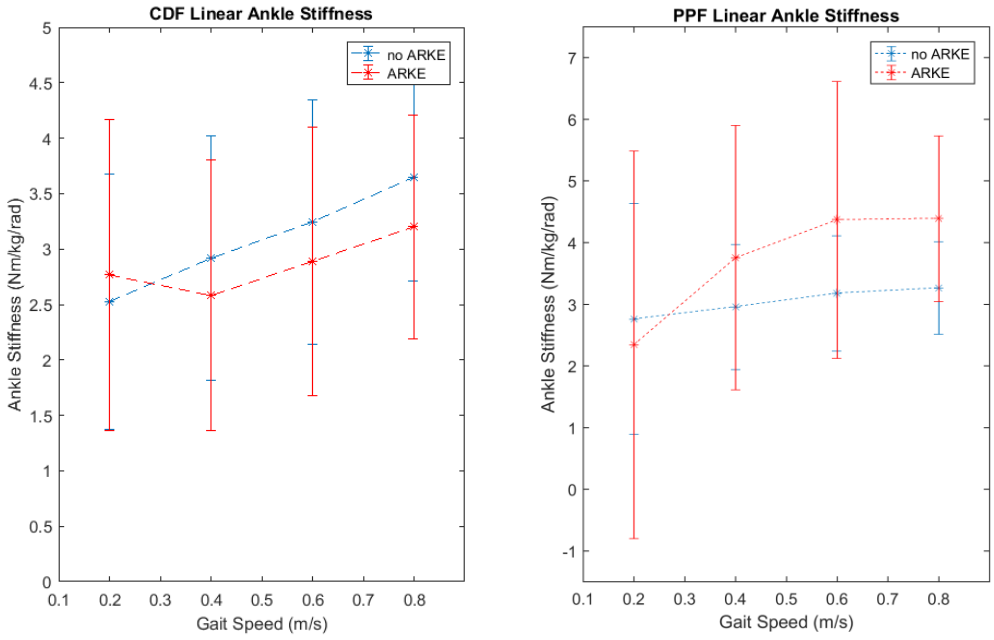

Figure 4-4 Linear ankle stiffness coefficients during CDF (left) and PPF (right) for four speeds when wearing ARKE or not wearing ARKE.

Mean quadratic term coefficients estimated by quadratic regression showed no significant differences across any conditions (Table 4-2). Although, CDF and PPF with-ARKE ankle quadratic angle term coefficients were slightly greater than without-ARKE. Quadratic ankle angle term coefficients were also greater for PPF than CDF, but not significantly, with quadratic ankle angle term coefficients in CDF increasing with speed but not in PPF. For with ARKE, in both CDF and PPF phases, the quadratic coefficients tended to increase with speed while the linear coefficient tended to decrease in magnitude with increasing speed, suggesting the non-linear elastic behavior of the ankle becomes more pronounced with increasing walking speed.

Table 4-2 Mean quadratic regression equations for CDF and PPF phase with and without ARKE. θ is ankle angle.

Speed (m/s)	CDF		PPF	
	ARKE	***No ARKE***	***ARKE***	***No ARKE***
0.2	$1.82\ \theta^2 + 2.83\ \theta - 0.13$	$-2.33\ \theta^2 + 3.30\ \theta + 0.05$	$18.50\ \theta^2 - 3.12\ \theta + 0.15$	$5.51\ \theta^2 + 1.39\ \theta + 0.04$
0.4	$3.51\ \theta^2 + 1.82\ \theta + 0.05$	$2.69\ \theta^2 + 2.50\ \theta + 0.11$	$19.17\ \theta^2 - 2.68\ \theta + 0.15$	$10.05\ \theta^2 + 0.46\ \theta + 0.14$
0.6	$5.72\ \theta^2 + 1.61\ \theta + 0.08$	$3.82\ \theta^2 + 2.67\ \theta + 0.14$	$18.82\ \theta^2 - 2.27\ \theta + 0.17$	$9.38\ \theta^2 + 1.03\ \theta + 0.16$
0.8	$7.71\ \theta^2 + 1.31\ \theta + 0.10$	$5.18\ \theta^2 + 2.88\ \theta + 0.12$	$13.61\ \theta^2 - 0.28\ \theta + 0.12$	$6.22\ \theta^2 + 2.06\ \theta + 0.23$

Mean work absorbed by the ankle during CDF phase was significantly less when wearing ARKE compared to without-ARKE and was different for each speed, whether with or without ARKE. Ankle work with-ARKE was not significantly different than without-ARKE for 0.6 m/s and 0.8 m/s. However, ankle work absorbed during CDF increased with speed for both ARKE conditions (Figure 4-6).

Work done by the ankle during PPF phase was significantly greater without-ARKE than with-ARKE. For both ARKE conditions, ankle work significantly increased with speed.

Mean total ankle work produced during stance phase was significantly less with-ARKE than without-ARKE, for all speeds. Total ankle work was significantly greater for 0.8m/s than all other speeds. Total work was negative for all conditions, except when not wearing ARKE and walking at 0.8 m/s (Table 4-3, Figure 4-5).

Table 4-3 Mean and total ankle work (J/kg) for CDF and PDF phases for with and without ARKE. SD in brackets.

Speed (m/s)	W_{CDF}		W_{PPF}		$W_{total=CDF+PPF}$	
	ARKE	***No ARKE***	***ARKE***	***No ARKE***	***ARKE***	***No ARKE***
0.2	-0.07 (0.04)	-0.08 (0.04)	0.01 (0.03)	0.07 (0.04)	-0.05 (0.05)	-0.02 (0.04)
0.4	-0.11 (0.04)	-0.11 (0.04)	0.06 (0.05)	0.10 (0.05)	-0.05 (0.05)	-0.02 (0.05)
0.6	-0.14 (0.04)	-0.14 (0.05)	0.09 (0.06)	0.13 (0.05)	-0.05 (0.05)	-0.01 (0.06)
0.8	-0.16 (0.05)	-0.15 (0.05)	0.14 (0.06)	0.18 (0.04)	-0.02 (0.05)	0.02 (0.06)

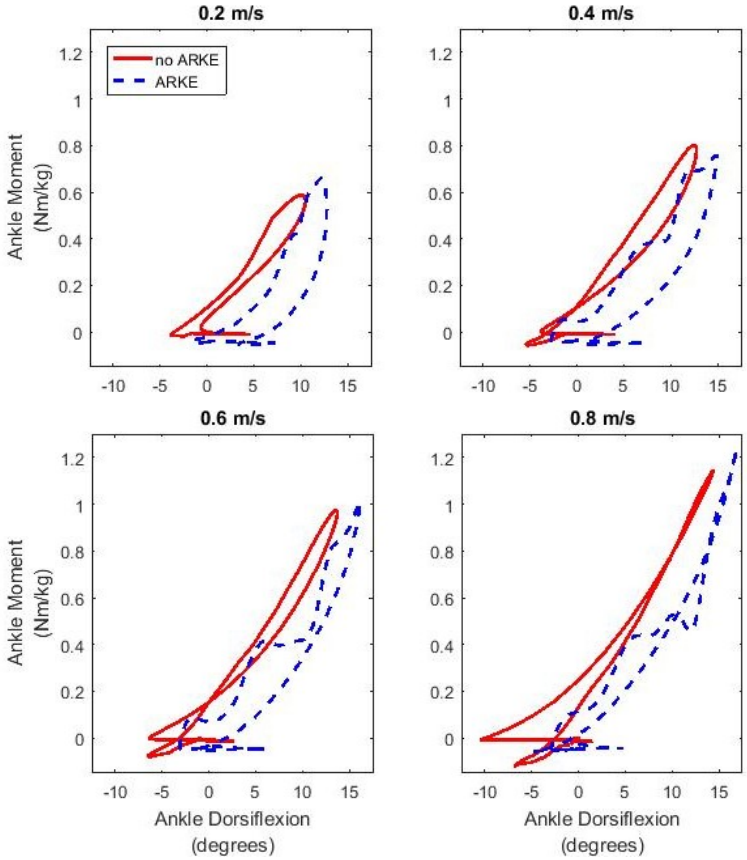

Figure 4-5 Mean ankle moment-displacement for with-ARKE (dashed blue line) and without-ARKE (solid red line) for four walking speeds. Area inside the curve is net ankle work.

For both CDF and PPF phases with ARKE, mean R^2 values for quadratic regressions were significantly greater than linear regressions. R^2 values increased significantly with speed for PPF phase, except between 0.6 and 0.8 m/s, but not for CDF (Table 4-4). Similarly, mean RMSE values were significantly lower for quadratic regressions compared to linear regressions.

Table 4-4 Mean R^2 and RMSE for linear and quadratic regression estimation of ankle quasi-stiffness by walking speed, with ARKE, for CDF and PPF phases. SD in brackets.

Speed (m/s)	Linear CDF		Quadratic CDF		Linear PPF		Quadratic PPF	
	R²	***RMSE***	***R²***	***RMSE***	***R²***	***RMSE***	***R²***	***RMSE***
0.2	0.64 (0.22)	0.16 (0.05)	0.74 (0.19)	0.13 (0.05)	0.50 (0.29)	0.13 (0.09)	0.65 (0.28)	0.10 (0.07)
0.4	0.70 (0.20)	0.15 (0.05)	0.75 (0.19)	0.13 (0.05)	0.81 (0.19)	0.12 (0.07)	0.90 (0.16)	0.07 (0.05)
0.6	0.70 (0.17)	0.19 (0.06)	0.75 (0.16)	0.17 (0.05)	0.87 (0.14)	0.13 (0.06)	0.94 (0.12)	0.07 (0.05)
0.8	0.70 (0.13)	0.22 (0.07)	0.76 (0.12)	0.19 (0.06)	0.91 (0.09)	0.14 (0.07)	0.96 (0.06)	0.08 (0.05)

For all conditions, mean R^2 values were greater and mean RMSE were lower for without-ARKE compared with-ARKE (Table 4-5).

Table 4-5 Mean R^2 and RMSE for linear and quadratic regression estimation of ankle quasi-stiffness by walking speeds, without ARKE, for CDF and PPF phases. SD in brackets

Speed (m/s)	Linear CDF		Quadratic CDF		Linear PPF		Quadratic PPF	
	R²	***RMSE***	***R²***	***RMSE***	***R²***	***RMSE***	***R²***	***RMSE***
0.2	0.80 (0.19)	0.08 (0.04)	0.88 (0.13)	0.06 (0.04)	0.91 (0.11)	0.05 (0.03)	0.96 (0.10)	0.03 (0.02)
0.4	0.93 (0.07)	0.07 (0.03)	0.97 (0.04)	0.04 (0.02)	0.93 (0.05)	0.07 (0.04)	0.99 (0.02)	0.03 (0.02)
0.6	0.94 (0.05)	0.07 (0.03)	0.98 (0.03)	0.04 (0.02)	0.94 (0.06)	0.08 (0.05)	0.99 (0.02)	0.02 (0.03)
0.8	0.95 (0.04)	0.08 (0.03)	0.99 (0.01)	0.04 (0.02)	0.96 (0.03)	0.08 (0.04)	1.00 (0.01)	0.02 (0.02)

Maximum ankle dorsiflexion was significantly greater for with- ARKE than without-ARKE, whereas maximum plantar flexion was significantly greater without-ARKE. Peak dorsiflexion and plantarflexion both increased with speed. Maximum ankle moments were significantly greater with-ARKE and increased with speed. However, maximum ankle power was significantly greater without-ARKE for all speeds and also increased significantly with speed (Table 4-6, Figure 4-7).

Table 4-6 Mean maximum ankle dorsiflexion, plantarflexion, moment, and power by walking speed with-ARKE and without-ARKE. SD in brackets

Speed (m/s)	Dorsiflexion (°)		Plantarflexion (°)		Moment (Nm/kg)		Power (W/kg)	
	ARKE	***No ARKE***	***ARKE***	***No ARKE***	***ARKE***	***No ARKE***	***ARKE***	***No ARKE***
0.2	15.07 (3.36)	12.24 (2.38)	4.77 (5.28)	7.65 (5.76)	0.91 (0.28)	0.67 (0.19)	0.14 (0.11)	0.23 (0.11)
0.4	16.25 (3.67)	13.84 (2.49)	5.90 (5.56)	9.15 (5.89)	0.99 (0.25)	0.86 (0.20)	0.45 (0.31)	0.55 (0.22)
0.6	17.01 (3.75)	14.59 (2.48)	6.71 (4.66)	10.30 (4.89)	1.22 (0.24)	1.03 (0.18)	0.90 (0.45)	1.08 (0.37)
0.8	17.40 (3.80)	14.92 (2.58)	7.20 (4.98)	12.64 (5.57)	1.41 (0.22)	1.19 (0.15)	1.50 (0.60)	1.82 (0.46)

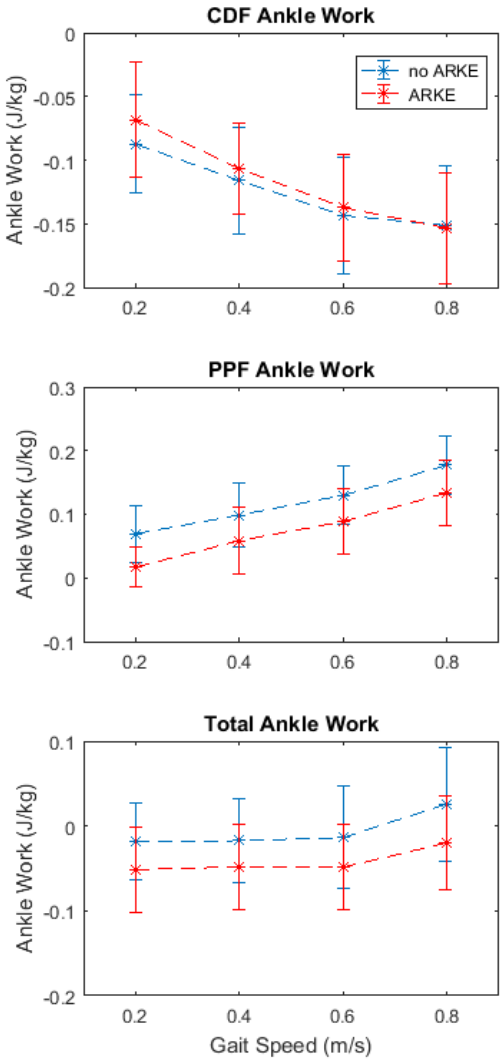

Figure 4-6 Ankle work during CDF, PPF, and total work done by the ankle for four slow walking speeds, with and without ARKE.

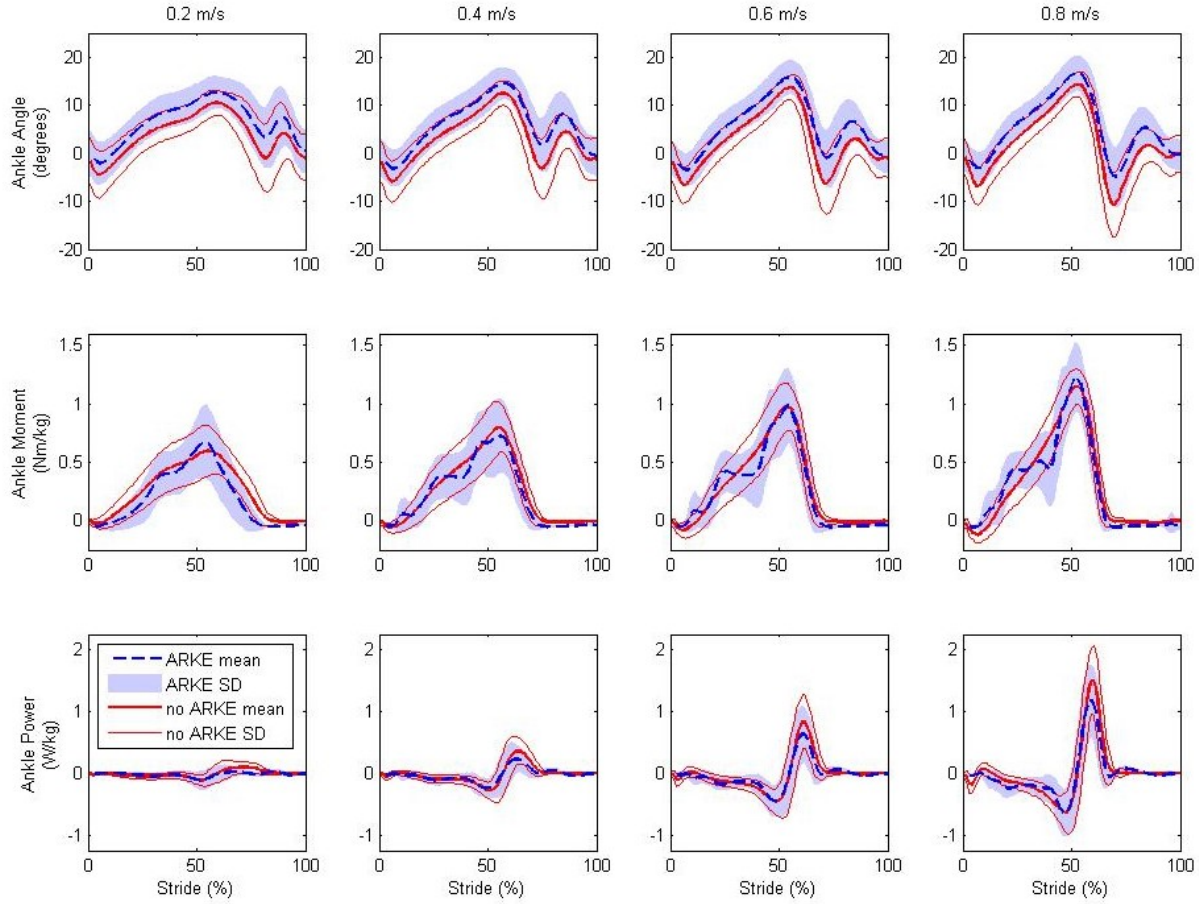

Figure 4-7 Mean ankle angle (dorsiflexion is positive), moment, and power for with-ARKE (dashed line with shaded area SD) and without-ARKE (solid line with thin solid line SD) for four walking speeds.

4.6 Discussion

This research presented a full body model of humans wearing the ARKE exoskeleton, driven by able-bodied very slow walking kinematics, and evaluated ARKE biomimetic ankle mechanics capable of reproducing realistic able-bodied slow walking motion. Characterizing biomimetic ankle mechanics for the ARKE enabled informed design recommendations for an improved LEPE ankle.

With-ARKE, linear ankle quasi-stiffness estimations were significantly different across all gait phases. Ankle quasi-stiffness increased with speed across CPF, CDF, PPF, significantly differing during PPF phase. To accommodate changes in stiffness across gait phase and speed, a biomimetic ankle design should incorporate variable-stiffness, capable of changing stiffness depending on gait phase and gait speed. Resistance to plantar flexion in early stance was very low (0.30 Nm/kg/rad) and essentially non-existent during swing while resistance to dorsiflexion was much greater in CDF (2.98 Nm/kg/rad) and even greater during PPF (3.87 Nm/kg/rad). Changes in order of magnitude

between resistance to plantar flexion and dorsiflexion imply the need for an asymmetrical-resistance ankle design.

Interestingly, with-ARKE ankle quasi-stiffness during CPF was significantly less than without-ARKE. This should be considered in design since too much plantar flexion resistance during early stance would prevent early foot flat, reducing base of support, COP progression, and stability. With respect to plantar flexion resistance design requirements, if swing phase quasi-stiffness is lower than CPF quasi-stiffness, but still resists plantarflexion to enable toe clearance, situations where foot-ground contact occurs during swing would be more easily accommodated. This lower ankle stiffness would provide more compliance between the foot and ground obstacles, reducing contact forces and potentially reducing stumble severity.

Ankle quasi-stiffness in CDF phase was greater without-ARKE but in PPF phase was greater with-ARKE. This suggests that inertial changes induced by attaching the ARKE require the ankle to function less as a break during CDF and provide a more solid base for PPF push-off.

Biomimetic ARKE ankle dorsiflexion resisting quasi-stiffness values were much greater than the current ankle design, which provides no dorsiflexion resistance up to 15° where a mechanical hard stop is engaged. Mean linear quasi-stiffness values for CDF and PPF phases, for all speeds, were very close to the literature, although these values were smaller for both with and without ARKE conditions, probably due to realistic slower speeds used in this study [37]–[39].

For quadratic regressions, high variance in CPF phase quadratic term coefficients were likely due to the phase's short period, leading to small samples. In fact, some cases at 0.2 m/s and 0.4 m/s had no CPF phase. Quadratic term coefficients for CDF phase increased with speed and were greater with-ARKE. PPF quadratic term coefficients did not vary with speed and were also consistently greater with-ARKE. This differed from the purely linear results during CDF where ARKE quasi-stiffness coefficients were lower than modeling without-ARKE, suggesting that quadratic regression captured an important property of ARKE ankle stiffness that linear regression suppressed.

For both CDF and PPF phases, quadratic regression R^2 values were significantly greater with significantly lower RMSE than linear regressions for all speeds. Incorporating a quadratic elastic element in an ankle design would thus be more successful at mimicking biological motion. However, R^2 values were significantly smaller for with-ARKE than without-ARKE for CDF. Additionally, with-ARKE R^2 for CDF was smaller than PPF. This is likely due to with-ARKE fluctuations in ankle moment during single leg support (Figure 4-7). With-ARKE model data from [153] also showed fluctuations during the same gait cycle periods, occurring simultaneously in anterior-posterior GRF and COP position. The cause of these fluctuations was not GRF predictions errors because these fluctuations occurred during single stance and not the indeterminate double support phase. These

ankle moment fluctuations were likely related to inertial changes from adding the ARKE to the human model which altered the mass distribution of the legs and torso and changed the COM position. Maximum contralateral swing foot acceleration occurred at the same time as the ankle moment fluctuations, suggesting that altered swing limb inertia with-ARKE caused the ankle moment fluctuations. In addition, the ankle moment fluctuations were more severe for faster speeds compared to slower speeds (i.e., greater swing limb accelerations), as would be expected if the changes were due to altered inertial properties from adding the exoskeleton to the human body.

In addition to reducing the goodness of fit of the linear and quadratic regressions for CDF, this transient modulation of ankle moment may not be energetically optimal. Indeed, biomimetic motion from able-bodied individuals may not be optimal for the with-ARKE condition since adding the ARKE altered the system's inertia enough to create compensatory fluctuations in ankle moment. If the swing limb was modelled as a simple point-mass pendulum, the length of the pendulum modelling the human leg compared to length of the pendulum modelling the with-ARKE leg would be different (due to different COM positions), leading to a different natural frequency. The length of the inverted pendulum that models the whole body during stance would also be different between the human without-ARKE and human with-ARKE (due to different mass distribution and COM positions), leading to different natural dynamics and different optimized kinematics [154]. Since the modulated ankle moment was likely related to swing limb inertia, the modelled with-ARKE swing limb may have been forced to swing too fast, or faster than its natural frequency. These unnatural swing dynamics may have induced energy inefficiencies at the with-ARKE hip or knee joint [104]. However, if these potentially energetically sub-optimal kinematics are caused by relatively high swing limb accelerations and angular velocity, this energy inefficiency may be offset by greater dynamic stability since increased swing limb velocity increases stability of biped walkers in the sagittal plane [155], [156].

Despite this potentially suboptimal motion, total measured ankle work during stance was significantly lower for the with-ARKE ankle than for human only ankle. This was mostly due to less work produced during PPF phase in the with-ARKE model. While the human ankle produced net positive work during stance for the highest speed (0.8 m/s), the ARKE ankle only had to absorb energy. Therefore a fully passive ARKE ankle design could meet biomimetic requirements. The lower PPF work at the ARKE ankle may be due in part to the altered inertial properties of adding the ARKE, although maximum with-ARKE ankle moment was higher than without-ARKE. The likely cause of the lower PPF work was lower ARKE ankle angle range of motion within the same period, since the ARKE ankle joint center was superior to the natural ankle joint center. Reduced ankle work may have been compensated for by increased knee or hip work.

Average maximum dorsiflexion was greater for with-ARKE than without-ARKE. In fact, with-ARKE maximum dorsiflexion was consistently greater than the current ARKE maximum of 15°. Maximum plantar flexion was significantly reduced in the with-ARKE model. These results were in part due to the COM correction increasing dorsiflexion and reduced ARKE ankle range of motion. The greater peak ankle moments in the ARKE model may have been due to GRF prediction model errors since peak moments occurred near double support phase, although the differences may also have been due to altered system inertia from the addition of the ARKE. Meanwhile, peak power in the with-ARKE model was reduced, possibly due to the reduced ankle rotation (and thus reduced angular velocity given the same period) and lower terminal stance ankle moment. Lower terminal stance phase ankle moment could have been caused by GRF prediction model errors or the altered system dynamics of the with-ARKE model.

In summary, results from this research suggest that a biomimetic ankle design for a LEPE with similar inertial distribution should: be mechanically passive, be capable of changing stiffness for different gait phases and different speeds, use a quadratic elastic element for dorsiflexion resistance with average stiffness of approximately 4.5 Nm/kg/rad, permit a slightly larger sagittal ankle range of motion (10° plantarflexion to 20° dorsiflexion), and be capable of providing moments up to 1.5 Nm/kg and peak power up to 2 W/kg.

Limitations of the study should be noted. Healthy slow walking human motion was assumed to be optimal for LEPE walking; however, as mentioned previously, the altered system inertia from the addition of the ARKE may cause substantially altered natural dynamics. To validate this approach, total net joint work should be compared across different swing limb frequencies with-ARKE and without-ARKE to determine if optimal swing limb frequency differs between conditions. In addition, only quasi-stiffness was measured, not true ankle stiffness. Adding additional parameters to the regression (e.g., ankle angular velocity, acceleration, adjusting for user height) could improve regression accuracy. Furthermore, this ARKE model assumed biomimetic knee and hip joints. An optimal ankle joint on a system with non-biomimetic knee and hip joints may be quite different from an optimal ankle joint on a system with biomimetic knee and hip joints. To simulate paraplegia, all muscles were removed with human joints having zero stiffness but, in reality, impedance still exists in the lower limb joints and soft tissues [157], [158]. Therefore ARKE estimated ankle stiffness may be slightly overestimated. Ankle mechanics in frontal plane were ignored but should also be studied and taken into consideration for biomimetic ankle design.

4.7 Conclusion

This research presented mechanical joint requirements for realistic slow walking of a biomimetic lower extremity powered exoskeleton ankle. Requirements were obtained by analyzing moment-displacement curves from a validated full body model of a real LEPE attached to a human-model driven by healthy slow walking kinematics. Results suggested that a passive variable stiffness ankle with quadratic elastic spring element could achieve biomimetic ankle requirements for a LEPE, with stiffness changing across gait phases and walking speeds. Such a biomimetic ankle design could reduce crutch use and, allow spinal cord injured LEPE users to walk faster and longer, thus improving quality of life and increasing potential health benefits of using LEPE.

Chapter 5: Thesis conclusions and future work

This thesis developed and implemented two models of a full 3D combined human-ARKE LEPE system that included interactions between human and LEPE. The first model was a biomimetic model that used 3D marker data from able-bodied individuals not wearing a LEPE to drive the model. The second model was a SCI model that included crutches and was kinematically driven by 3D marker data from SCI individuals wearing the ARKE. Both models were validated by comparing predicted and measured GRF and COP. Additionally, using the biomimetic model, biomimetic LEPE ankle mechanical requirements for slow walking were determined. Using these requirements, biomimetic ankle design recommendations were made for the ARKE. An ankle design implementing these requirements should increase LEPE user walking speed, stability, and reduce overuse of crutches, thus reducing user fatigue and increasing LEPE time of use. Conclusions for each thesis objective and hypothesis are presented below.

5.1 Objective 1: Evaluate validity of biomimetic model of combined human musculoskeletal model and LEPE for different slow walking speeds

5.1.1 Hypothesis 1: The model will satisfactorily replicate measured GRF

For the biomimetic model, correlations between measured and predicted values were high to very high for all GRF and moderate to high for all COP, across all walking speeds, with relatively small RMSE. Thus, the model satisfactorily replicated measured GRF. As expected, vertical GRF had the strongest correlations, considering the large signal to noise ratio compared to medio-lateral and anterior-posterior GRF, while COP correlations were lowest.

5.1.2 Hypothesis 2: Accuracy of ground reaction force model will increase with walking speed

Predictions were expected to be more accurate for increasing walking speed because DST decreases with increasing speed, and DST would presumably cause greater model errors from the indeterminacy that arises with both feet in contact with the ground. For medio-lateral and anterior-poster GRF, correlations modestly increased between measured and predicted values with increasing walking speed; however, this was not the case for vertical GRF or COP. Vertical GRF remained constant from 0.4 to 0.8 m/s but COP correlations generally decreased with walking speed. This unexpected decrease in accuracy with speed may be due to the altered inertial properties of the

human with-ARKE versus human without-ARKE conditions. Effects of the different inertial distributions would be more pronounced with increasing speed.

5.2 Objective 2: Simulate motion of SCI participants using the ARKE and further validate the model by measuring accuracy of predicted GRF

5.2.1 Hypothesis: The model will satisfactorily replicate ground reaction forces

Although accuracy of predicted GRF and COP were lower for the SCI model than for the biomimetic model, correlations were acceptable and RMSE were low. In fact, vertical GRF correlations were very high and medio-lateral GRF, anterior-posterior GRF, and anterior-posterior COP correlations were moderate. Only medio-lateral COP correlations were weak, as expected since medio-lateral COP is a very low amplitude signal. This COP measure could be improved with GRF prediction nodes closer to the medial and lateral edges of the LEPE feet. In general, lower correlations were expected since this model was driven by the slowest walking speeds (~0.14m/s), thus having the longest DST, and instrumented crutch data may have also contributed errors.

5.3 Objective 3: Determine biomimetic ankle requirements of the ARKE LEPE for different walking speeds

5.3.1 Hypothesis 1: Ankle will absorb net energy for all speeds and ankle stiffness will increase with walking speed

As expected, simulations demonstrated that even for the highest walking speed (0.8 m/s) the biomimetic ARKE ankle absorbed net energy, meaning an actively powered ankle is unnecessary to replicate biological function in the ARKE LEPE for slow walking. Biomimetic ankle quasi-stiffness generally increased with speed for CPF, CDF, and PPF, as expected, although the increase with speed was only significant during PPF phase.

5.3.2 Hypothesis 2: Quadratic regression will provide a significantly better estimation of biomimetic ankle quasi-stiffness

As expected, the quadratic regression significantly outperformed the linear regression in terms of R^2 value and RMSE for predicting ankle moment. R^2 values increased by an average of 0.08

for CDF and PPF phases. These results suggest a biomimetic LEPE ankle design should incorporate quadratic elastic elements for dorsiflexion resistance, instead of linear resistive elements.

5.3.3 Hypothesis 3: Ankle mechanical properties while wearing the ARKE will be different from human only ankle properties when not wearing ARKE

Adding the ARKE to the human model drastically changed ankle joint mechanical properties. The with-ARKE model had lower CDF phase quasi-stiffness but higher PPF phase quasi-stiffness, compared to without-ARKE. Thus, a biomimetic ankle on a LEPE should act as less of a brake during CDF and allow greater forward momentum, but provide a more stable lever arm for PPF phase compared to the biological ankle. The biomimetic ARKE ankle had a general tendency to promote forward progression and impede movement less than the biological ankle.

Other differences included the lower PPF positive work in the with-ARKE model compared to without-ARKE. This implies that the biomimetic LEPE ankle is even less in need of active actuation than the biological ankle.

Maximum dorsiflexion was also increased in the with-ARKE model because of the COM correction. This increase in dorsiflexion implies the need for greater ARKE ankle ROM.

5.4 Summary of realistic slow walking requirements for a biomimetic LEPE ankle

The following realistic slow walking requirements for biomimetic ARKE LEPE ankle are derived from results in chapter 4:

- Mechanically passive
- Capable of changing stiffness in different gait phases and for different speeds
- Use a quadratic elastic element for dorsiflexion resistance with average stiffness of approximately 4.5 Nm/kg/rad
- Permit a larger sagittal ankle range of motion (10° plantarflexion to 20° dorsiflexion) than currently allowed by the ARKE
- Capable of providing moments up to 1.5 Nm/kg
- Capable of providing peak power up to 2 W/kg

5.5 Future work

This research presented a validated model of a biomimetic LEPE and a real LEPE with crutches, as well as characterized biomimetic LEPE ankle mechanics using the first model. These models open the door to many new research opportunities.

A possible design that may fit requirements from the previous section includes a quadratic dorsiflexion resisting spring in series with a proportional clutch and a weaker parallel dorsiflexion biasing spring for toe-clearance and controlled plantar flexion. The Endolite Elan prosthetic foot is an example of this type of strategy (i.e., hydraulic cylinder with variable valve opening sizes is used as a proportional clutch), as well as the orthotic design presented in [60], although without the proportional aspect. The proportional clutch controls the overall joint stiffness, with the maximum stiffness occurring when the clutch is 100% engaged, where the joint stiffness becomes equal to the quadratic spring stiffness. A design schematic is presented in Figure 5-1.

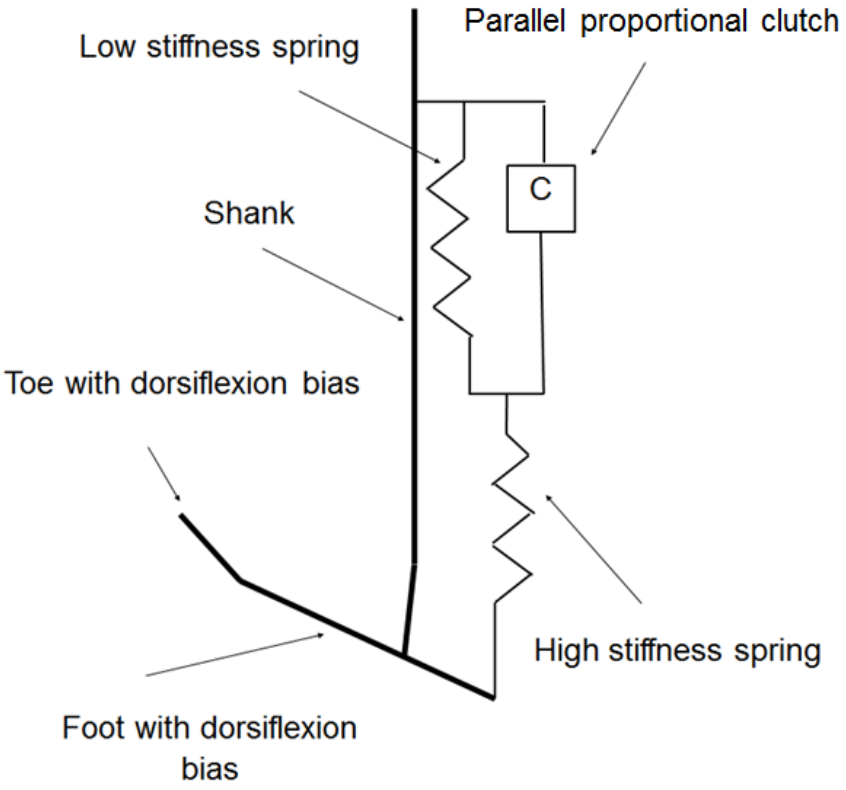

Figure 5-1 Schematic of design principles for biomimetic LEPE ankle.

5.5.1 Improvements to models

- A rigorous sensitivity analysis of predicted GRF model parameters and their effect on calculated GRF should be undertaken with a small subset of participants to further improve the model.
- LEPE-human interaction modelling could be more detailed, especially the connection between the ARKE pelvis segment and the human trunk. Model accuracy could be compared against a new model that includes more detailed interactions, such as a contact model that includes friction forces.
- Predictive GRF nodes should be placed closer to the edges of the feet to increase base of support.
- Even for complete SCI simulation, lower limb muscles should be included in the model with contractile element set to zero in order to include passive muscle and tendon components.
- Contact forces accuracy between ARKE and human should be evaluated by comparing measured values to actual measured values. Predicted vertical reaction forces for human foot and ARKE foot could be compared with measured F-Scan (Tekscan, Inc) pressure data.
- Implementing a metatarsophalangeal joint into the model would be extremely useful for testing ARKE ankle-foot complex design ideas.
- Allowing internal/external rotation at the knee and ankle could also improve model accuracy.

5.5.2 SCI model research

- The SCI model can be used to evaluate different crutch strategies and their effect on upper limb loading for various activities of daily living.
- The SCI model could also be used when comparing different ARKE designs, measuring outcomes such as maximal muscles activity, predicted metabolic rate, joint moments, use of crutches etc.

5.5.3 Biomimetic model research

- Biomimetic LEPE hip and knee joint mechanics should be characterized for realistic slow walking.
- Biomimetic LEPE joint mechanics should be characterized for other activities of daily living; such as, sit-to-stand, stair climbing, ramp climbing, quiet standing, and turning.

- LEPE joint designs can be modelled and optimized using either model. Generally, the model does not predict motion, thus designs would be optimized to reduce LEPE joint actuator power. However the model can be modified to predict motion over a short period.
- Literature suggests bi-articulate elastic elements could increase biped efficiency and speed. Such elements could be modelled and tested on the biomimetic and SCI model. One particularly interesting idea from the literature, for better efficiency and speed, would be a tri-articulate Achilles tendon like design that would span the knee, ankle, and metatarsophalangeal joints.
- A parameter optimization study should be undertaken to determine optimized design parameters for the proposed design configuration. Two potential designs are proportional clutch and on/off clutch. Parameters would include spring moment arm, spring stiffness coefficients, and clutch timing for the on/off clutch design, or clutch resistance timing for the proportional clutch design.
- Evaluating the difference between walking kinematics of optimized human with-LEPE motion versus human without-LEPE motion could be undertaken by generating kinematics with different swing limb velocity, or recording walking data with different stride times and measuring total joint work as an outcome.

References

[1] E. N. Marieb and K. Hoehn, *Human Anatomy & Physiology*, 9th edition. Boston: Pearson, 2012.

[2] "Anatomy: Foot/Ankle." [Online]. Available: http://www.drwolgin.com/Pages/footankleanat.aspx. [Accessed: 30-Jun-2015].

[3] J. Perry and J. M. Burnfield , *Gait Analysis: Normal and Pathological Function*, Second Edition edition. Thorofare, NJ: Slack Incorporated, 2010.

[4] J. Chen, S. Siegler, and C. D. Schneck, "The three-dimensional kinematics and flexibility characteristics of the human ankle and subtalar joint--Part II: Flexibility characteristics," *J. Biomech. Eng.*, vol. 110, no. 4, pp. 374–385, Nov. 1988.

[5] M. J. Shereff, F. J. Bejjani, and F. J. Kummer, "Kinematics of the first metatarsophalangeal joint.," *J. Bone Jt. Surg.*, vol. 68, no. 3, pp. 392–398, Mar. 1986.

[6] Donatelli, "Normal Biomechanics of the Foot and Ankle," *J. Orthop. Sports Phys. Ther.*, vol. 7, no. 3, pp. 91–95, Nov. 1985.

[7] "Gait - Physiopedia, universal access to physiotherapy knowledge." [Online]. Available: http://www.physio-pedia.com/Gait. [Accessed: 30-Jun-2015].

[8] M. Wisse, "Three additions to passive dynamic walking: actuation, an upper body, and 3d stability," *Int. J. Humanoid Robot.*, vol. 02, no. 04, pp. 459–478, Dec. 2005.

[9] S.H. Collins, "*Dynamic Walking Principles Applied to Human Gait*" Ph.D. dissertation, Mech Eng, Uni. of. Mich. Ann Arbor, 2008.

[10] T. McGeer, "Passive dynamic walking," *Int. J. Robot. Res.*, vol. 9, no. 2, pp. 62–82, Apr. 1990.

[11] D. Winter, "Human balance and posture control during standing and walking," *Gait Posture*, vol. 3, no. 4, pp. 193–214, Dec. 1995.

[12] M. Wisse, D. G. E. Hobbelen, R. J. J. Rotteveel, S. O. Anderson, and G. J. Zeglin, "Ankle springs instead of arc-shaped feet for passive dynamic walkers," in *2006 6th IEEE-RAS Int. Conf. Humanoid Robots*, 2006, pp. 110–116.

[13] M. T. Vanderpool, S. H. Collins, and A. D. Kuo, "Ankle fixation need not increase the energetic cost of human walking," *Gait Posture*, vol. 28, no. 3, pp. 427–433, Oct. 2008.

[14] M. Kim and S. H. Collins, "Once-per-step control of ankle-foot prosthesis push-off work reduces effort associated with balance during walking," *J. NeuroEngineering Rehabil.*, vol. 12, no. 1, Dec. 2015.

[15] M. Kim and S. H. Collins, “Step-to-Step Ankle Inversion/Eversion Torque Modulation Can Reduce Effort Associated with Balance,” *Front. Neurorobotics*, vol. 11, 2017.

[16] T. Chen, M. Kim, S. T. Del, and S. H. Collins, “Inversion-Eversion Stiffness of Ankle-Foot Prosthesis Affects Amputee’s Balance-Related Effort during Walking,” in *Proc. Dyn. Walk.*, 2015.

[17] Y. Jian, D. Winter, M. Ishac, and L. Gilchrist, “Trajectory of the body COG and COP during initiation and termination of gait,” *Gait Posture*, vol. 1, no. 1, pp. 9–22, Mar. 1993.

[18] A. Chang *et al.*, “The relationship between toe-out angle during gait and progression of medial tibiofemoral osteoarthritis,” *Ann. Rheum. Dis.*, vol. 66, no. 10, pp. 1271–1275, Oct. 2007.

[19] P. DeVita, J. Helseth, and T. Hortobagyi, “Muscles do more positive than negative work in human locomotion,” *J. Exp. Biol.*, vol. 210, no. 19, pp. 3361–3373, Oct. 2007.

[20] M. Ishikawa, P. V. Komi, M. J. Grey, V. Lepola, and G.-P. Bruggemann, “Muscle-tendon interaction and elastic energy usage in human walking,” *J. Appl. Physiol.*, vol. 99, no. 2, pp. 603–608, Aug. 2005.

[21] P. R. Cavanagh and P. V. Komi, “Electromechanical delay in human skeletal muscle under concentric and eccentric contractions,” *Eur. J. Appl. Physiol.*, vol. 42, no. 3, pp. 159–163, Nov. 1979.

[22] G. S. Sawicki, C. L. Lewis, and D. P. Ferris, “It pays to have a spring in your step:,” *Exerc. Sport Sci. Rev.*, vol. 37, no. 3, pp. 130–138, Jul. 2009.

[23] S. Song and H. Geyer, “The energetic cost of adaptive feet in walking,” in *2011 IEEE Int. Conf. Robot. Biomim. ROBIO*, 2011, pp. 1597–1602.

[24] S. Song, C. LaMontagna, S. H. Collins, and H. Geyer, “The effect of foot compliance encoded in the windlass mechanism on the energetics of human walking,” in *2013 35th Annu. Int. Conf. IEEE Eng. Med. Biol. Soc. EMBC*, 2013, pp. 3179–3182.

[25] H.-Y. K. Cheng, C.-L. Lin, H.-W. Wang, and S.-W. Chou, “Finite element analysis of plantar fascia under stretch—The relative contribution of windlass mechanism and Achilles tendon force,” *J. Biomech.*, vol. 41, no. 9, pp. 1937–1944, 2008.

[26] D. Laroche, T. Pozzo, P. Ornetti, C. Tavernier, and J. F. Maillefert, “Effects of loss of metatarsophalangeal joint mobility on gait in rheumatoid arthritis patients,” *Rheumatology*, vol. 45, no. 4, pp. 435–440, Apr. 2006.

[27] D. Tlalolini, C. Chevallereau, and Y. Aoustin, “Human-Like Walking: Optimal Motion of a Bipedal Robot With Toe-Rotation Motion,” *IEEEASME Trans. Mechatron.*, vol. 16, no. 2, pp. 310–320, Apr. 2011.

[28] R. R. Neptune, S. A. Kautz, and F. E. Zajac, “Contributions of the individual ankle plantar flexors to support, forward progression and swing initiation during walking,” *J. Biomech.*, vol. 34, no. 11, pp. 1387–1398, Nov. 2001.

[29] M. P. Kadaba, H. K. Ramakrishnan, and M. E. Wootten, “Measurement of lower extremity kinematics during level walking,” *J. Orthop. Res.*, vol. 8, no. 3, pp. 383–392, May 1990.

[30] S. H. Scott and D. A. Winter, “Talocrural and talocalcaneal joint kinematics and kinetics during the stance phase of walking,” *J. Biomech.*, vol. 24, no. 8, pp. 743–752, 1991.

[31] J. Zhu, Q. Wang, and L. Wang, “On the Design of a Powered Transtibial Prosthesis With Stiffness Adaptable Ankle and Toe Joints,” *IEEE Trans. Ind. Electron.*, vol. 61, no. 9, pp. 4797–4807, Sep. 2014.

[32] J. J. Eng and D. A. Winter, “Kinetic analysis of the lower limbs during walking: What information can be gained from a three-dimensional model?,” *J. Biomech.*, vol. 28, no. 6, pp. 753–758, Jun. 1995.

[33] A. H. Hansen, D. S. Childress, S. C. Miff, S. A. Gard, and K. P. Mesplay, “The human ankle during walking: implications for design of biomimetic ankle prostheses,” *J. Biomech.*, vol. 37, no. 10, pp. 1467–1474, Oct. 2004.

[34] K. Shamaei, M. Cenciarini, and A. M. Dollar, “On the mechanics of the ankle in the stance phase of the gait,” *Conf. Proc. Annu. Int. Conf. IEEE Eng. Med. Biol. Soc. IEEE Eng. Med. Biol. Soc. Annu. Conf.*, vol. 2011, pp. 8135–8140, 2011.

[35] M. L. Palmer, “Sagittal plane characterization of normal human ankle function across a range of walking gait speeds,” Thesis, Massachusetts Institute of Technology, 2002.

[36] R. B. Davis and P. A. DeLuca, “Gait characterization via dynamic joint stiffness,” *Gait Posture*, vol. 4, no. 3, pp. 224–231, May 1996.

[37] Z. Safaeepour, A. Esteki, F. T. Ghomshe, and N. A. A. Osman, “Quantitative analysis of human ankle characteristics at different gait phases and speeds for utilizing in ankle-foot prosthetic design,” *Biomed. Eng. OnLine*, vol. 13, no. 1, pp. 1–13, Mar. 2014.

[38] K. Shamaei, G. S. Sawicki, and A. M. Dollar, “Estimation of quasi-stiffness and propulsive work of the human ankle in the stance phase of walking,” *PLoS ONE*, vol. 8, no. 3, p. e59935, Mar. 2013.

[39] E. J. Rouse, L. J. Hargrove, E. J. Perreault, and T. A. Kuiken, “Estimation of human ankle impedance during the stance phase of walking,” *IEEE Trans. Neural Syst. Rehabil. Eng. Publ. IEEE Eng. Med. Biol. Soc.*, vol. 22, no. 4, pp. 870–878, Jul. 2014.

[40] E. J. Rouse, R. D. Gregg, L. J. Hargrove, and J. W. Sensinger, “The difference between stiffness and quasi-stiffness in the context of biomechanical modeling,” *IEEE Trans. Biomed. Eng.*, vol. 60, no. 2, pp. 562–568, Feb. 2013.

[41] M. L. Latash and V. M. Zatsiorsky, “Joint stiffness: Myth or reality?,” *Hum. Mov. Sci.*, vol. 12, no. 6, pp. 653–692, Dec. 1993.

[42] E. H. Melis, R. Torres-Moreno, H. Barbeau, and E. D. Lemaire, “Analysis of assisted-gait characteristics in persons with incomplete spinal cord injury,” *Spinal Cord*, vol. 37, no. 6, pp. 430–439, Jun. 1999.

[43] B. A. Slavens, N. Bhagchandani, M. Wang, P. A. Smith, and G. F. Harris, “An upper extremity inverse dynamics model for pediatric Lofstrand crutch-assisted gait,” *J. Biomech.*, vol. 44, no. 11, pp. 2162–2167, Jul. 2011.

[44] R. G. Pringle, “Crutch walker’s shoulder,” *J. R. Soc. Med.*, vol. 94, no. 10, pp. 554–554, Oct. 2001.

[45] S. Lal, “Premature degenerative shoulder changes in spinal cord injury patients,” *Spinal Cord*, vol. 36, no. 3, pp. 186–189, Mar. 1998.

[46] J. C. Bayley, T. P. Cochran, and C. B. Sledge, “The weight-bearing shoulder. The impingement syndrome in paraplegics.,” *J. Bone Jt. Surg.*, vol. 69, no. 5, pp. 676–678, Jun. 1987.

[47] H. Gellman, I. Sie, and R. L. Waters, “Late complications of the weight-bearing upper extremity in the paraplegic patient,” *Clin. Orthop.*, no. 233, pp. 132–135, Aug. 1988.

[48] “eLEGS - An Exoskeleton That Helps The Paraplegic Walk Upright,” *UpcomingTechnology.ORG*. [Online]. Available: http://www.upcomingtechnology.org/elegs/. [Accessed: 21-May-2015].

[49] “Exoskeleton technology: an interview with Larry Jasinski, CEO, ARGO Medical Technologies,” *News-Medical.net*. [Online]. Available: http://www.news-medical.net/news/20121212/Exoskeleton-technology-an-interview-with-Larry-Jasinski-CEO-ARGO-Medical-Technologies.aspx. [Accessed: 21-May-2015].

[50] “Indego exoskeleton by Parker Hannifin for rehabilitating spinal cord injury and stroke patients,” *DamnGeeky*. [Online]. Available: http://www.damngeeky.com/2013/01/23/8502/indego-exoskeleton-by-parker-hannifin-for-rehabilitating-spinal-cord-injury-and-stroke-patients.html. [Accessed: 21-May-2015].

[51] “CYBERDYNE.” [Online]. Available: http://www.cyberdyne.jp/. [Accessed: 09-Jun-2015].

[52] “REX Exoskeleton: Robotic Legs For Paraplegics Patients | The Cool Gadgets - Quest for The Coolest Gadgets.” [Online]. Available: http://thecoolgadgets.com/rex-exoskeleton-robotic-legs-for-paraplegics-patients/. [Accessed: 21-May-2015].

[53] D. R. Louie, J. J. Eng, and T. Lam, “Gait speed using powered robotic exoskeletons after spinal cord injury: a systematic review and correlational study,” *J. NeuroEngineering Rehabil.*, vol. 12, no. 1, p. 1, Oct. 2015.

[54] H. Kawamoto and Y. Sankai, “Power assist method based on Phase Sequence and muscle force condition for HAL,” *Adv. Robot.*, vol. 19, no. 7, pp. 717–734, Jan. 2005.

[55] A. Tsukahara, Y. Hasegawa, and Y. Sankai, “Standing-up motion support for paraplegic patient with Robot Suit HAL,” in *IEEE Int. Conf. Rehabil. Robot. 2009 ICORR 2009*, 2009, pp. 211–217.

[56] A. W. Andrews, S. A. Chinworth, M. Bourassa, M. Garvin, D. Benton, and S. Tanner, “Update on distance and velocity requirements for community ambulation,” *J. Geriatr. Phys. Ther. 2001*, vol. 33, no. 3, pp. 128–134, Sep. 2010.

[57] W. van Dijk, H. van der Kooij, and E. Hekman, “A passive exoskeleton with artificial tendons: Design and experimental evaluation,” in *2011 IEEE Int. Conf. Rehabil. Robot. ICORR*, 2011, pp. 1–6.

[58] C. J. Walsh, K. Endo, and H. Herr, “A quasi-passive leg exoskeleton for load-carrying augmentation,” *Int. J. Humanoid Robot.*, vol. 04, no. 03, pp. 487–506, Sep. 2007.

[59] A. Valiente, “Design of a Quasi-Passive Parallel Leg Exoskeleton to Augment Load Carrying for Walking,” Aug. 2005.

[60] M. B. Wiggin, G. S. Sawicki, and S. H. Collins, “An exoskeleton using controlled energy storage and release to aid ankle propulsion,” in *2011 IEEE Int. Conf. Rehabil. Robot. ICORR*, 2011, pp. 1–5.

[61] S. H. Collins, M. B. Wiggin, and G. S. Sawicki, “Reducing the energy cost of human walking using an unpowered exoskeleton,” *Nature*, vol. advance online publication, Apr. 2015.

[62] K. E. Gordon and D. P. Ferris, “Learning to walk with a robotic ankle exoskeleton,” *J. Biomech.*, vol. 40, no. 12, pp. 2636–2644, 2007.

[63] P. Malcolm, W. Derave, S. Galle, and D. De Clercq, “A Simple Exoskeleton That Assists Plantarflexion Can Reduce the Metabolic Cost of Human Walking,” *PLoS ONE*, vol. 8, no. 2, p. e56137, Feb. 2013.

[64] K. Kim, C.-H. Yu, M. Yu, G.-Y. Jeong, D.-Y. Ko, and T.-K. Kwon, “The effects of a powered ankle exoskeleton for plantarflexion torque assistance for the elderly,” *Int. J. Precis. Eng. Manuf.*, vol. 14, no. 2, pp. 307–315, Jan. 2013.

[65] L. M. Mooney, E. J. Rouse, and H. M. Herr, “Autonomous exoskeleton reduces metabolic cost of human walking during load carriage,” *J. NeuroEngineering Rehabil.*, vol. 11, no. 1, p. 80, May 2014.

[66] S. Wang, W. van Dijk, and H. van der Kooij, “Spring uses in exoskeleton actuation design,” in *2011 IEEE Int. Conf. Rehabil. Robot. ICORR*, 2011, pp. 1–6.

[67] R. Versluys, P. Beyl, M. Van Damme, A. Desomer, R. Van Ham, and D. Lefeber, “Prosthetic feet: State-of-the-art review and the importance of mimicking human ankle–foot biomechanics,” *Disabil. Rehabil. Assist. Technol.*, vol. 4, no. 2, pp. 65–75, Jan. 2009.

[68] A. E. Ferris, J. M. Aldridge, C. A. Rábago, and J. M. Wilken, “Evaluation of a Powered Ankle-Foot Prosthetic System During Walking,” *Arch. Phys. Med. Rehabil.*, vol. 93, no. 11, pp. 1911–1918, Nov. 2012.

[69] G. A. Alan R De Asha, “Mechanical and physiological energetics when using an Echelon hydraulic ankle-foot device in unilateral trans-tibial amputees,” 2014.

[70] A. R. De Asha, L. Johnson, R. Munjal, J. Kulkarni, and J. G. Buckley, “Attenuation of centre-of-pressure trajectory fluctuations under the prosthetic foot when using an articulating hydraulic ankle attachment compared to fixed attachment,” *Clin. Biomech.*, vol. 28, no. 2, pp. 218–224, Feb. 2013.

[71] I. Sedki and R. Moore, “Patient evaluation of the Echelon foot using the Seattle Prosthesis Evaluation Questionnaire,” *Prosthet. Orthot. Int.*, vol. 37, no. 3, pp. 250–254, Jun. 2013.

[72] D. Moser *et al.*, *Prosthetic ankle joint mechanism*. 2007.

[73] “echelonVT | Feet | Prosthetic Product Catalogue | Endolite North America.” [Online]. Available: http://www.endolite.com/products/echelonvt. [Accessed: 16-Jun-2015].

[74] M. L. van der Linden, N. Twiste, and S. V. S. Rithalia, “The biomechanical effects of the inclusion of a torque absorber on trans-femoral amputee gait, a pilot study,” *Prosthet. Orthot. Int.*, vol. 26, no. 1, pp. 35–43, Jan. 2002.

[75] P. L. Weiss, R. E. Kearney, and I. W. Hunter, “Position dependence of ankle joint dynamics—I. Passive mechanics,” *J. Biomech.*, vol. 19, no. 9, pp. 727–735, 1986.

[76] D. Moser, N. Stech, J. McCarthy, G. Harris, S. Zahedi, and A. McDougall, “Analysis of ankle kinetics and energy consumption with an advanced microprocessor controlled ankle foot prosthesis.,” 2012.

[77] C.-Y. Ko *et al.*, “Comparison of ankle angle adaptations of prosthetic feet with and without adaptive ankle angle during level ground, ramp, and stair ambulations of a transtibial amputee: A pilot study,” *Int. J. Precis. Eng. Manuf.*, vol. 15, no. 12, pp. 2689–2693, Dec. 2014.

[78] S. H. Collins and A. D. Kuo, “Recycling Energy to Restore Impaired Ankle Function during Human Walking,” *PLoS ONE*, vol. 5, no. 2, p. e9307, Feb. 2010.

[79] A. D. Segal *et al.*, “The effects of a controlled energy storage and return prototype prosthetic foot on transtibial amputee ambulation,” *Hum. Mov. Sci.*, vol. 31, no. 4, pp. 918–931, Aug. 2012.

[80] S. K. Au, J. Weber, and H. Herr, “Powered Ankle–Foot Prosthesis Improves Walking Metabolic Economy,” *IEEE Trans. Robot.*, vol. 25, no. 1, pp. 51–66, Feb. 2009.

[81] S. K. Au and H. Herr, “Powered ankle-foot prosthesis,” *IEEE Robot. Autom. Mag.*, vol. 15, no. 3, pp. 52–59, Sep. 2008.

[82] J. Hitt, T. Sugar, M. Holgate, R. Bellman, and K. Hollander, “Robotic transtibial prosthesis with biomechanical energy regeneration,” *Ind. Robot Int. J.*, vol. 36, no. 5, pp. 441–447, Aug. 2009.

[83] F. Sup, H. A. Varol, J. Mitchell, T. Withrow, and M. Goldfarb, “Design and control of an active electrical knee and ankle prosthesis,” in *2nd IEEE RAS EMBS Int. Conf. Biomed. Robot. Biomechatronics 2008 BioRob 2008*, 2008, pp. 523–528.

[84] P. Cherelle, K. Junius, V. Grosu, H. Cuypers, B. Vanderborght, and D. Lefeber, “The AMP-Foot 2.1 : actuator design, control and experiments with an amputee,” *Robotica*, vol. 32, no. Special Issue 08, pp. 1347–1361, Dec. 2014.

[85] “MANTA Product Development, Inc. - Cambridge, Massachusetts - Industrial Design, Engineering, Strategic Consulting.” [Online]. Available: http://www.designdirectory.com/MANTA/iWalk-Biom. [Accessed: 17-Jun-2015].

[86] P. Malcolm, R. E. Quesada, J. M. Caputo, and S. H. Collins, “The influence of push-off timing in a robotic ankle-foot prosthesis on the energetics and mechanics of walking,” *J. NeuroEngineering Rehabil.*, vol. 12, no. 1, Dec. 2015.

[87] J. M. Caputo and S. H. Collins, “Prosthetic ankle push-off work reduces metabolic rate but not collision work in non-amputee walking,” *Sci. Rep.*, vol. 4, Dec. 2014.

[88] J. E. Shaw, C. H. van Schie, A. L. Carrington, C. A. Abbott, and A. J. Boulton, “An analysis of dynamic forces transmitted through the foot in diabetic neuropathy.,” *Diabetes Care*, vol. 21, no. 11, pp. 1955–1959, Nov. 1998.

[89] J. A. Blaya and H. Herr, “Adaptive control of a variable-impedance ankle-foot orthosis to assist drop-foot gait,” *IEEE Trans. Neural Syst. Rehabil. Eng.*, vol. 12, no. 1, pp. 24–31, Mar. 2004.

[90] "The Evolution of Powered Orthotic Technology | American Academy of Orthotists & Prosthetists." [Online]. Available: http://www.oandp.org/AcademyTODAY/2014Oct/3.asp. [Accessed: 18-Jun-2015].

[91] L. Yang, D. N. Condie, M. H. Granat, J. P. Paul, and D. I. Rowley, "Effects of joint motion constraints on the gait of normal subjects and their implications on the further development of hybrid FES orthosis for paraplegic persons," *J. Biomech.*, vol. 29, no. 2, pp. 217–226, Feb. 1996.

[92] D. J. J. Bregman, M. M. van der Krogt, V. de Groot, J. Harlaar, M. Wisse, and S. H. Collins, "The effect of ankle foot orthosis stiffness on the energy cost of walking: A simulation study," *Clin. Biomech.*, vol. 26, no. 9, pp. 955–961, Nov. 2011.

[93] P. J. Greene and M. H. Granat, "A knee and ankle flexing hybrid orthosis for paraplegic ambulation," *Med. Eng. Phys.*, vol. 25, no. 7, pp. 539–545, Sep. 2003.

[94] E. S. Park, C. I. Park, H. J. Chang, J. E. Choi, and D. S. Lee, "The effect of hinged ankle-foot orthoses on sit-to-stand transfer in children with spastic cerebral palsy," *Arch. Phys. Med. Rehabil.*, vol. 85, no. 12, pp. 2053–2057, Dec. 2004.

[95] Q. Huang *et al.*, "A high stability, smooth walking pattern for a biped robot," in *1999 IEEE Int. Conf. Robot. Autom. 1999 Proc.*, 1999, vol. 1, pp. 65–71 vol.1.

[96] J. H. Park and H. Chung, "ZMP compensation by online trajectory generation for biped robots," in *1999 IEEE Int. Conf. Syst. Man Cybern. 1999 IEEE SMC 99 Conf. Proc.*, 1999, vol. 4, pp. 960–965 vol.4.

[97] J. H. Park and O. Kwon, "Reflex control of biped robot locomotion on a slippery surface," in *IEEE Int. Conf. Robot. Autom. 2001 Proc. 2001 ICRA*, 2001, vol. 4, pp. 4134–4139 vol.4.

[98] J. Pratt, P. Dilworth, and G. Pratt, "Virtual model control of a bipedal walking robot," in *1997 IEEE Int. Conf. Robot. Autom. 1997 Proc.*, 1997, vol. 1, pp. 193–198 vol.1.

[99] J. Pratt and G. Pratt, "Intuitive control of a planar bipedal walking robot," in *1998 IEEE Int. Conf. Robot. Autom. 1998 Proc.*, 1998, vol. 3, pp. 2014–2021 vol.3.

[100] J. E. Pratt, "Exploiting inherent robustness and natural dynamics in the control of bipedal walking robots," Jun. 2000.

[101] S. H. Collins, M. Wisse, and A. Ruina, "A Three-Dimensional Passive-Dynamic Walking Robot with Two Legs and Knees," *Int. J. Robot. Res.*, vol. 20, no. 7, pp. 607–615, Jul. 2001.

[102] Q. Wang, Y. Huang, and L. Wang, "Passive dynamic walking with flat feet and ankle compliance," *Robotica*, vol. 28, no. 03, pp. 413–425, May 2010.

[103] F. Asano, M. Yamakita, and K. Furuta, “Virtual passive dynamic walking and energy-based control laws,” in *2000 IEEERSJ Int. Conf. Intell. Robots Syst. 2000 IROS 2000 Proc.*, 2000, vol. 2, pp. 1149–1154 vol.2.

[104] S. H. Collins and A. Ruina, “A bipedal walking robot with efficient and human-like gait,” in *Proc. 2005 IEEE Int. Conf. Robot. Autom. 2005 ICRA 2005*, 2005, pp. 1983–1988.

[105] J. M. Hausdorff, P. L. Purdon, C. K. Peng, Z. Ladin, J. Y. Wei, and A. L. Goldberger, “Fractal dynamics of human gait: stability of long-range correlations in stride interval fluctuations,” *J. Appl. Physiol.*, vol. 80, no. 5, pp. 1448–1457, May 1996.

[106] M. J. Kurz and N. Stergiou, “Hip Actuations Can be Used to Control Bifurcations and Chaos in a Passive Dynamic Walking Model,” *J. Biomech. Eng.*, vol. 129, no. 2, pp. 216–222, Dec. 2006.

[107] E. Ott, C. Grebogi, and J. A. Yorke, “Controlling chaos,” *Phys. Rev. Lett.*, vol. 64, no. 11, pp. 1196–1199, Mar. 1990.

[108] T. Shinbrot, C. Grebogi, E. Ott, and J. A. Yorke, “Using small perturbations to control chaos,” *Nature*, vol. 363, pp. 411–417, Jun. 1993.

[109] J. Starrett and R. Tagg, “Control of a Chaotic Parametrically Driven Pendulum,” *Phys. Rev. Lett.*, vol. 74, no. 11, pp. 1974–1977, Mar. 1995.

[110] P. Shi, Y. Zhang, and X. Yang, “Lower extremity exoskeleton control and stability analysis based on virtual prototyping technique,” in *2008 Int. Conf. Comput. Sci. Softw. Eng.*, 2008, vol. 1, pp. 1131–1134.

[111] H. Yali and W. Xingsong, “Kinematics analysis of lower extremity exoskeleton,” in *2008 Chin. Control Decis. Conf.*, 2008, pp. 2837–2842.

[112] Y. Liao, C. Wang, X. Wu, F. Lu, P. Wang, and S. Cai, “On the mechanical design and control of a self-adaptive exoskeleton chair,” in *2015 IEEE Int. Conf. Inf. Autom.*, 2015, pp. 937–942.

[113] D. Pan, F. Gao, Y. Miao, and R. Cao, “Co-simulation research of a novel exoskeleton-human robot system on humanoid gaits with fuzzy-PID/PID algorithms,” *Adv. Eng. Softw.*, vol. 79, pp. 36–46, Jan. 2015.

[114] Y. Li, X. Guan, Y. Tong, and C. Xu, “Design and simulation study of the translational-knee lower extremity exoskeleton,” *Mechanics*, vol. 21, no. 3, pp. 207–213, Jun. 2015.

[115] H. Baskar and S. M. R. Nadaradjane, “Minimization of metabolic cost of muscles based on human exoskeleton modeling: a simulation,” *Int. J. Biomed. Eng. Sci.*, vol. 3, no. 4, p. 9, Oct. 2016.

[116] T. K. Uchida, A. Seth, S. Pouya, C. L. Dembia, J. L. Hicks, and S. L. Delp, "Simulating ideal assistive devices to reduce the metabolic cost of running," *PLOS ONE*, vol. 11, no. 9, p. e0163417, Sep. 2016.

[117] M. S. Shourijeh, M. Jung, S.-T. Ko, M. McGrath, N. Stech, and M. Damsgaard, "Simulating physiological discomfort of exoskeletons using musculoskeletal modelling," *Gait Posture*, Jul. 2017.

[118] C. Meijneke, W. van Dijk, and H. van der Kooij, "Achilles: An autonomous lightweight ankle exoskeleton to provide push-off power," in *5th IEEE RASEMBS Int. Conf. Biomed. Robot. Biomechatronics*, 2014, pp. 918–923.

[119] C. F. Ong, J. L. Hicks, and S. L. Delp, "Simulation-based design for wearable robotic systems: an optimization framework for enhancing a standing long jump," *IEEE Trans. Biomed. Eng.*, vol. 63, no. 5, pp. 894–903, May 2016.

[120] P. Agarwal, P. H. Kuo, R. R. Neptune, and A. D. Deshpande, "A novel framework for virtual prototyping of rehabilitation exoskeletons," in *2013 IEEE 13th Int. Conf. Rehabil. Robot. ICORR*, 2013, pp. 1–6.

[121] P. Agarwal, M. S. Narayanan, L.-F. Lee, F. Mendel, and V. N. Krovi, "Simulation-based design of exoskeletons using musculoskeletal analysis," pp. 1357–1364, Jan. 2010.

[122] F. Ferrati, R. Bortoletto, and E. Pagello, "Virtual modelling of a real exoskeleton constrained to a human musculoskeletal model," in *Biomimetic and Biohybrid Systems*, N. F. Lepora, A. Mura, H. G. Krapp, P. F. M. J. Verschure, and T. J. Prescott, Eds. Springer Berlin Heidelberg, 2013, pp. 96–107.

[123] Y. Zhu, J. Cui, and J. Zhao, "Biomimetic design and biomechanical simulation of a 15-DOF lower extremity exoskeleton," in *2013 IEEE Int. Conf. Robot. Biomim. ROBIO*, 2013, pp. 1119–1124.

[124] K. Cho, Y. Kim, M. Jung, and K. Lee, "Analysis and evaluation of a combined human - exoskeleton model under two different constraints condition," *Proc. Int. Summit Hum. Simul.*, pp. 1–10, 2012.

[125] X. Guan, L. Ji, R. Wang, and W. Huang, "Optimization of an unpowered energy-stored exoskeleton for patients with spinal cord injury," in *2016 38th Annu. Int. Conf. IEEE Eng. Med. Biol. Soc. EMBC*, 2016, pp. 5030–5033.

[126] S. E. Oh, A. Choi, and J. H. Mun, "Prediction of ground reaction forces during gait based on kinematics and a neural network model," *J. Biomech.*, vol. 46, no. 14, pp. 2372–2380, Sep. 2013.

[127] R. R. Neptune, I. C. Wright, and A. J. V. D. Bogert, “A method for numerical simulation of single limb ground contact events: application to heel-toe running,” *Comput. Methods Biomech. Biomed. Engin.*, vol. 3, no. 4, pp. 321–334, Jan. 2000.

[128] F. C. Anderson and M. G. Pandy, “Dynamic optimization of human walking,” *J. Biomech. Eng.*, vol. 123, no. 5, pp. 381–390, May 2001.

[129] S. R. Hamner, A. Seth, K. M. Steele, and S. L. Delp, “A rolling constraint reproduces ground reaction forces and moments in dynamic simulations of walking, running, and crouch gait,” *J. Biomech.*, vol. 46, no. 10, pp. 1772–1776, Jun. 2013.

[130] R. Fluit, M. S. Andersen, S. Kolk, N. Verdonschot, and H. F. J. M. Koopman, “Prediction of ground reaction forces and moments during various activities of daily living,” *J. Biomech.*, vol. 47, no. 10, pp. 2321–2329, Jul. 2014.

[131] Y. Jung, M. Jung, K. Lee, and S. Koo, “Ground reaction force estimation using an insole-type pressure mat and joint kinematics during walking,” *J. Biomech.*, vol. 47, no. 11, pp. 2693–2699, Aug. 2014.

[132] Y. Jung, M. Jung, J. Ryu, S. Yoon, S.-K. Park, and S. Koo, “Dynamically adjustable foot-ground contact model to estimate ground reaction force during walking and running,” *Gait Posture*, vol. 45, pp. 62–68, Mar. 2016.

[133] M. Talaty, A. Esquenazi, and J. E. Briceno, “Differentiating ability in users of the ReWalk(TM) powered exoskeleton: an analysis of walking kinematics,” *IEEE Int. Conf. Rehabil. Robot. Proc.*, vol. 2013, p. 6650469, Jun. 2013.

[134] K. Witte, J. Zhang, R. Jackson, and S. Collins, “Design of two lightweight, high-bandwidth torque-controlled ankle exoskeletons,” *Proc. IEEE Int. Conf. Robot. Autom. ICRA*, pp. 1223–1228, Oct. 2014.

[135] D. P. Ferris, J. M. Czerniecki, and B. Hannaford, “An ankle-foot orthosis powered by artificial pneumatic muscles,” *J. Appl. Biomech.*, vol. 21, no. 2, pp. 189–197, May 2005.

[136] “anybodytech.com: Frontpage.” [Online]. Available: https://www.anybodytech.com/. [Accessed: 19-Mar-2017].

[137] C. F. Runge, C. L. Shupert, F. B. Horak, and F. E. Zajac, “Ankle and hip postural strategies defined by joint torques,” *Gait Posture*, vol. 10, no. 2, pp. 161–170, Oct. 1999.

[138] E. H. Sinitski, E. D. Lemaire, and N. Baddour, “Evaluation of motion platform embedded with dual belt treadmill instrumented with two force plates,” *J. Rehabil. Res. Dev.*, vol. 52, no. 2, pp. 221–234, 2015.

[139] L. M. Giangregorio *et al.*, “Body weight supported treadmill training in acute spinal cord injury: impact on muscle and bone,” *Spinal Cord*, vol. 43, no. 11, pp. 649–657, Nov. 2005.

[140] K. T. Ragnarsson, “Functional electrical stimulation after spinal cord injury: current use, therapeutic effects and future directions,” *Spinal Cord*, vol. 46, no. 4, pp. 255–274, Apr. 2008.

[141] L. Noreau, P. Proulx, L. Gagnon, M. Drolet, and M. T. Laramée, “Secondary impairments after spinal cord injury: a population-based study,” *Am. J. Phys. Med. Rehabil.*, vol. 79, no. 6, pp. 526–535, Dec. 2000.

[142] D. S. Ditor *et al.*, “The effects of body-weight supported treadmill training on cardiovascular regulation in individuals with motor-complete SCI,” *Spinal Cord*, vol. 43, no. 11, pp. 664–673, Nov. 2005.

[143] A. L. Hicks and K. A. M. Ginis, “Treadmill training after spinal cord injury: It’s not just about the walking,” *J. Rehabil. Res. Dev.*, vol. 45, no. 2, pp. 241–248, Mar. 2008.

[144] M. Talaty, A. Esquenazi, and J. E. Briceno, “Differentiating ability in users of the ReWalkTM powered exoskeleton: An analysis of walking kinematics,” in *2013 IEEE Int. Conf. Rehabil. Robot. ICORR*, 2013, pp. 1–5.

[145] V. Agrawal, R. Gailey, I. A. Gaunaurd, C. O’Toole, and A. A. Finnieston, “Comparison between microprocessor-controlled ankle/foot and conventional prosthetic feet during stair negotiation in people with unilateral transtibial amputation,” *J. Rehabil. Res. Dev.*, vol. 50, no. 7, pp. 941–950, 2013.

[146] L. Fradet, M. Alimusaj, F. Braatz, and S. I. Wolf, “Biomechanical analysis of ramp ambulation of transtibial amputees with an adaptive ankle foot system,” *Gait Posture*, vol. 32, no. 2, pp. 191–198, Jun. 2010.

[147] M. Ishikawa, P. V. Komi, M. J. Grey, V. Lepola, and G.-P. Bruggemann, “Muscle-tendon interaction and elastic energy usage in human walking,” *J. Appl. Physiol.*, vol. 99, no. 2, pp. 603–608, Aug. 2005.

[148] K. Endo, D. Paluska, and H. Herr, “A quasi-passive model of human leg function in level-ground walking,” in *2006 IEEERSJ Int. Conf. Intell. Robots Syst.*, 2006, pp. 4935–4939.

[149] G. S. Sawicki and D. P. Ferris, “Mechanics and energetics of level walking with powered ankle exoskeletons,” *J. Exp. Biol.*, vol. 211, no. Pt 9, pp. 1402–1413, May 2008.

[150] L. M. Mooney and H. M. Herr, “Biomechanical walking mechanisms underlying the metabolic reduction caused by an autonomous exoskeleton,” *J. NeuroEngineering Rehabil.*, vol. 13, p. 4, Jan. 2016.

[151] M. Kim and S. H. Collins, “Once-per-step control of ankle-foot prosthesis push-off work reduces effort associated with balance during walking,” *J. NeuroEngineering Rehabil.*, vol. 12, no. 1, Dec. 2015.

[152] F. Ferrati, R. Bortoletto, and E. Pagello, “Virtual modelling of a real exoskeleton constrained to a human musculoskeletal model,” in *Biomim. Biohybrid Syst.*, 2013, pp. 96–107.

[153] B. Fournier, E. Lemaire, A. J. J. Smith, and M. Doumit, “Modelling and simulation of a lower extremity powered exoskeleton,” *Be Submitt. IEEE Trans. Neural Syst. Rehabil. Eng.*, Oct. 2017.

[154] R. C. Browning, J. R. Modica, R. Kram, and A. Goswami, “The effects of adding mass to the legs on the energetics and biomechanics of walking,” *Med. Sci. Sports Exerc.*, vol. 39, no. 3, pp. 515–525, Mar. 2007.

[155] M. Wisse, “Three additions to passive dynamic walking: actuation, an upper body, and 3d stability,” *Int. J. Humanoid Robot.*, vol. 02, no. 04, pp. 459–478, Dec. 2005.

[156] T. McGeer, “Passive dynamic walking,” *Int. J. Robot. Res.*, vol. 9, no. 2, pp. 62–82, Apr. 1990.

[157] A. Roy *et al.*, “Measurement of Human Ankle Stiffness Using the Anklebot,” in *2007 IEEE 10th Int. Conf. Rehabil. Robot.*, 2007, pp. 356–363.

[158] P. L. Weiss, R. E. Kearney, and I. W. Hunter, “Position dependence of ankle joint dynamics—I. Passive mechanics,” *J. Biomech.*, vol. 19, no. 9, pp. 727–735, 1986.